Ultrafast and highly selective gold recovery with high capture capacity from electronic-waste by upconversional silsesquioxane-based hybrid luminescent aerogel

Qingzheng Wang,[ab] Masafumi Unno *[b] and Hongzhi Liu *[a]

[a] International Center for Interdisciplinary Research and Innovation of Silsesquioxane Science, Key Laboratory of Special Functional Aggregated Materials, Ministry of Education, School of Chemistry and Chemical Engineering, Shandong University, 27 Shanda Nanlu, Jinan, 250100, China.

[b] Department of Chemistry and Chemical Biology, Graduate School of Science and Technology, Gunma University, Kiryu, 376-8515, Japan.

Supplementary Text

Materials

Unless otherwise indicated, all reagents and materials were obtained from commercial suppliers without purification. Thiol-attached chitosan and 4-(dicyanomethylene)-2,6-bis(4-(carbazolo-9-yl))phenyl)-4H-pyran (CZ-B-DCM) were synthesized from the previous reports.[1,2] 1,2-dichloroethane was dried by distillation over calcium hydride under reflux prior to use.

Synthesis of 4-Carbazolo-phenyl aldehyde

In an oven-dried flask was added 9H-Carbazole (2.006 g, 12 mmol), 4-Bromobenzaldehyde (2.78 g, 15 mmol), CuI (0.38 g, 2 mmol) and K_2CO_3 (2.5 g, 18 mmol) in DMF (16 mL) under argon. The mixture was stirred for 30 min at room temperature and subsequently heated at 140 °C for 24 h. After cooling to room temperature, the mixture was filtered and washed with dichloromethane. The product was obtained by rotary evaporation, and purified by column chromatography (silica gel, ethyl acetate: n-Hexane = 1:30). The product was dried under vacuum at 70 °C for 24 h. 4-carbazolo-phenyl aldehyde was obtained as a light-yellow powder (2.28 g). Yield: 70%.

Synthesis of 4-(dicyanomethylene)-2,6-bis(4-(carbazolo-9-yl))phenyl)-4H-pyran (CZ-B-DCM)

4-Carbazolo-phenyl aldehyde (0.271 g, 1 mmol) and 2-(2,6-dimethyl-4H-pyran-4-ylidene)-malononitrile (0.086 g, 0.5 mmol,) were dissolved into dried CH_3CN (20.0 mL). The mixtures were heated to refluxing and maintain 24 h under the catalysis of piperidine. After removing solvents under reduced pressure, recrystallization was conducted in acetonitrile. CZ-B-DCM was obtained as an orange powder with 90% yield, and the structure was confirmed by the following methods (figs. S28 and S29). ^{1}H NMR (400 MHz, (CD_2Cl_2), δ (ppm): 8.08 (d, J = 8 Hz, 4 H), 7.81 (d, J = 8 Hz, 4 H), 7.64 (m, 6 H), 7.43 (d, J = 8 Hz, 4 H), 7.37 (t, J = 8 Hz, 4 H), 7.24 (t, J=8 Hz, 4H), 6.86 (t, J=16Hz, 2H), 6.72 (s, 2 H). ^{13}C NMR (100MHz, CD_2Cl_2), δ (ppm): 60.47, 107.82, 109.93, 115.19, 119.34, 120.48, 120.71, 123.78, 126.28, 127.33, 129.46, 133.69, 136.84, 139.58, 140.56, 155.78, 158.28.

Material characterization

^{1}H NMR (400 MHz) spectra of CZ-B-DCM were recorded by Bruker Avance spectrometer, and dissolved in CD_2Cl_2 at room temperature with tetramethylsilane (TMS) as the internal standard. ^{13}C NMR (100 MHz) spectra of CZ-B-DCM were recorded by Bruker Avance spectrometer, and dissolved in CD_2Cl_2 at room temperature. Fourier-transform infrared (FTIR) spectra were recorded with a Bruker Tensor 27 spectrophotometer with a disc of KBr from 4000 to 400 cm^{-1} at a resolution of 4 cm^{-1}. The data were treated with OPUS spectroscopy software version 6. Solid-state ^{13}C cross-polarization/magic-angle-spinning (CP/MAS) NMR and ^{29}Si MAS NMR spectra were performed using a Bruker Avance-500 NMR spectrometer operating at a magnetic field strength of 9.4 T. The resonance frequencies were 125 and 99 MHz for ^{13}C NMR and ^{29}Si NMR, respectively. A Chemagnetics 5 mm triple-resonance MAS probe was used to acquire ^{13}C NMR and ^{29}Si NMR spectra. ^{29}Si MAS NMR spectra with high-power proton decoupling were recorded using a π/2 pulse length of 5 μs, a recycle delay of 120 s, and a spinning rate of 5 kHz. Powder X-ray diffraction (PXRD) was measured using a Riguku D/MAX 2550 diffractometer under Cu-Kα radiation, 40 kV, 200 mA with a 2θ range of 5–80° (scanning rate of 10°min^{-1}) at room temperature. Thermogravimetric Analyses (TGA) were conducted with a Mettler-Toledo SDTA-854 TGA system in nitrogen (100 mL min^{-1}) at a heating rate of 10 °C min^{-1} from 30 °C to 800 °C. Elemental analyses were performed using an Elementar EL III elemental analyzer. High-resolution transmission electron mi-croscopy (HR-TEM) experiments were recorded using a JEM 2100 electron microscope (JEOL, Japan) with an acceleration voltage of 200 kV. Field-emission scanning electron microscopy (FE-SEM) experiments were recorded with a HITACHI S4800 spectrometer. Fluorescent quantum yield was recorded from FLS920 under the excitation of 441 nm laser and $BaSO_4$ as blank reference. Fluorescence lifetime was measured by a FLS920 with time correlated single photo counting (TCSPC) method with 441 nm excited laser. The data was deconvoluted with the instrument response function, recorded by reduced light, and fitted multi-exponential function. XPS analysis of the solid samples was performed using Thermofish0er ESCALAB 250Xi spectrometer with monochromatized Al Kα radiation under ultrahigh vacuum ($<10^{-7}$ Pa). All binding energies were referenced to the C1s peak (284.6 eV) arising from carbon impurities. An electron spin resonance (ESR, JES-X320, Japan) spectrometer was used to characterize the ROS generated using 5, 5-dimethyl-L-pyrroline N-oxide (DMPO) as the spin trap reagent. Ultraviolet-visible diffuse reflectance spectra (UV-vis DRS) were recorded on a UV-vis spectrophotometer (Cary 5000, Agilent, America) with BaSO4 as a reflectance standard. Nitrogen adsorption-desorption isotherm measurements were performed with a Quadra Sorb SI apparatus at 77 K. The samples were degassed at 150 °C for 12 h prior to measurement. A sample of approximately 100 mg and UHP-grade nitrogen (99.999%) gas source were used in the nitrogen sorption measurements and collected with a Quantachrome Quadrasorb apparatus. BET surface areas were evaluated over a P/P_0 range from 0.01 to 0.20. Nonlocal density functional theory (NLDFT) pore-size distributions were confirmed by using the carbon/slit-cylindrical pore mode of the Quadrawin software. Mechanical tests were conducted on an electronic universal material-testing machine (3344, INSTRON, USA) equipped with a 500 N load cell. For the compressive test, the samples were shaped into cubic appearance (10 mm × 10 mm × 10 mm). The compressive rate was set 10 mm min^{-1}.

Stern–Volmer equation

$$I_0/I = K_{SV}[Q] + 1 \tag{1}$$

I_0 is the initial intensity of PCS-CZ-B-DCM and PCSs@chitosan suspension and I is the intensity with a given concentration of Au(III). [Q] is the molar concentration of Au(III) and K_{SV} is the quenching constant.

Calculating the limit of detection (LOD)

The limit of detection (LOD) for tetracycline was calculated using eq as follows

$$LOD = 3 \times \sigma/K \tag{2}$$

where σ represents the standard deviation of blank measurement, which was obtained by recording the fluorescence intensity of PCS-CZ-B-DCM and PCSs@chitosan suspension in aqueous solution ten times. The parameter K is the slope of fluorescence emission intensity excited at 490 nm versus the concentration of Au(III).

Adsorption experiments

General procedures

In a typical adsorption experiment, 5 mg of adsorbents were mixed with 20 mL of 200 mg L^{-1} Au(III) solution. Hydrochloric acid was used to adjust the pH. The experiment was carried out using a 300 W Xenon arc lamp as illuminant. After reaching adsorption equilibrium, the solid was isolated via filtration with 0.22 μm membrane. The concentration of the gold ions in the solution before and after adsorption was detected by Graphite Furnace atomic absorption spectroscopy (TAS-990).

Adsorption isotherms

The specific adsorption capacities onto adsorbents were determined based on the following formula:

$$Q_e = \frac{(C_0 - C_e) \times V}{m} \tag{3}$$

where Q_e (mg g^{-1}) is the equilibrium adsorption capacities, C_0 and C_e (mg L^{-1}) are the initial concentration and the residual or equilibrium concentration, respectively. V (L) is the volume of the aqueous solution and m (g) is the mass of the adsorbent used.

Adsorption equilibrium and kinetics

The adsorption equilibrium isotherm and relevant parameters were used to determine the adsorption mechanism and modeled using three models.

Langmuir model

$$\frac{C_e}{Q_e} = \frac{1}{Q_{max}} \times C_e + \frac{1}{K_L Q_{max}} \tag{4}$$

where C_e (mg L^{-1}) is the equilibrium concentration of solute, Q_e (mg g^{-1}) is the equilibrium adsorption capacity of adsorbent, Q_{max} (mg g^{-1}) is the saturated adsorption amount of adsorbent, and K_L(L g^{-1}) is the Langmuir adsorption constant.

Freundlich model

$$lnQ_e = lnK_F + \frac{1}{n} \times lnC_e \tag{5}$$

where C_e (mg L^{-1}) is the equilibrium concentration of solute, Q_e (mg g^{-1}) is the equilibrium adsorption capacity of adsorbent, K_F ($mg^{1-1/n}$ $L^{1/n}$ g^{-1}) and n are Freundlich isotherm constants, which refer to the capacity and intensity of the adsorption, respectively.

Temkin model

$$Q_e = \left(\frac{R \times T}{b}\right) \times lnC_e + \frac{R \times T \times lnK_T}{b} \tag{6}$$

where R, K_T and T are the gas constant (8.314 J/mol·K), equilibrium binding constant, and temperature (K).

Adsorption kinetic studies

5 mg of adsorbents were mixed with 20 mL of 200 ppm Au(III) solution for a different time. Hydrochloric acid was used to adjust the pH. The mixture was filtered, and the filtrate was collected and analyzed with Graphite Furnace atomic absorption spectroscopy (TAS-990) to determine the remaining Au(III).

The adsorption kinetics was explored using the pseudo-first order, pseudo-second order and intraparticle diffusion kinetic models, expressing as Eq. (7), Eq. (8), and Eq. (9):

$$\ln\left(Q_e - Q_t\right) = lnQ_e - K_1 t \tag{7}$$

$$\frac{t}{Q_t} = \frac{t}{Q_e} + \frac{1}{K_2 Q_e^2} \quad (8)$$

$$Q_t = K_i t^{1/2} + C \quad (9)$$

where Q_t (mg g^{-1}) and Q_e (mg g^{-1}) are the amounts of Au (III) adsorbed per gram adsorbent at time t and at equilibrium, respectively. K_1 and K_2 (g mg^{-1}·min) are the rate constants of the pseudo-first-order and pseudo-second-order model. K_i (mg g^{-1}·$min^{1/2}$) is the rate constant of intraparticle diffusion model. C is an indicator for expressing the boundary layer thickness.

Selective adsorption of Au(III)

The mixed solution (pH adjust with concentrated HNO_3) containing Au(III) (100 ppm), and 8 competitive metals (50 ppm) including Na(I), K(I), Cu(II), Mg(II), Cd(II), Cr(III), Fe(III), and Zn(II), was prepared. Adding 5 mg of adsorbents into 20 mL above as-prepared solution, and soaked for 1 h. After then the mixture was filtrated with 0.22 μm membrane, and the filtrate was analyzed by Graphite Furnace atomic absorption spectroscopy (TAS-990).

Gold adsorption from e-waste

The leaching solution was prepared by mixing 300 mL of distilled water with 7 mL of pyridine and NBS (4 g). The 20 CPUs was added to above prepared mixture to give the metal leaching solution. The metal leaching solution (300 ml) was pumped through PCSs@chitosan device (100 mg, 50 mg PCS-CZ-B-DCM equiv) using a 300 W Xenon arc lamp as illuminant at a flow rate of 150 mL min^{-1} and a device operation time of 30 min. Afterwards, the thiourea solution (100 ml, 1M) was pumped through PCSs@chitosan device and circulated for 2 hours to give yellow solution. The resulted yellow solution was reduced with $Na_2S_2O_5$ to give a black powder of gold. The powder was washed three times with 50 mL water and then air-dried. Then, 3 mg of borax was mixed into the powder as a stabilizer and the mixture was sintered at high temperature, and a molten golden yellow solid was obtained.

Desorption and recyclability

In a typical desorption experiment, after one run of adsorption, the thiourea solution (100ml, 1 M, pH = 2 adjust with concentrated HNO_3) was pumped through the used PCSs@chitosan device at a flow rate of 150 mL min-1 and a device operation time of 2 h. Afterwards, the ultra-pure water (100ml) was pumped through the used PCSs@chitosan device at a flow rate of 150 mL min^{-1} and a device operation time of 1 h. The used PCSs@chitosan device was transferred into a cold source for 12 h to produce and fix the ice crystals. The ice crystals were removed after freeze-drying at -50℃ for 24 h to give regenerated PCSs@chitosan, which were directly used for another adsorption experiment.

Electrochemical measurements

Electrochemical measurement was performed using three electrode systems on a CHI 760E electrochemical workstation in 0.1 M Na_2SO_4 solution. A platinum plate electrode and Ag/AgCl electrode were used as the counter electrode and the reference electrode, respectively. The working electrode was fabricated by mixing active materials, acetylene black and poly (vinylidene fluoride) (PVDF) in a weight ratio of 7:2:1. Then, this mixture was grounded in the presence of droplets of N-mathyl-2-pyrrolidone (NMP). After that, the black slurry was spread on a clean carbon fiber cloth by a doctor blade. Dry overnight at 60°C in a vacuum oven. The exposed geometric surface area was 1.0 cm^2.

DFT calculation

All the theoretical calculations were carried out using the Gaussian 16 software by density functional theory (DFT). To perform the quantum mechanics calculation for PCS-CZ-B-DCM, the model was constructed by extracting a unit from the PCS-CZ-B-DCM, and the boundaries of the truncated unit were capped with hydrogen atoms. The b3lyp functional and 6-311G(d) basis set were adopted for all calculations. The visualization of the orbitals was achieved using VMD software.

Cost analysis

Cost analysis of raw materials and electricity in PCSs@chitosan preparation process are presented in the Supporting Information, fig. S22, the detailed data are summarized in table S5, along with the corresponding calculated production energy. All data (price of electricity in Jinan, price of raw materials and gold price in China) were obtained in May, 2023. And all data were at the lab-scale. From fig. S22, the production cost for synthesis of 1 g PCSs@chitosan is around 244.466 CNY, and more than 95 % of which are spent on raw materials. Although this production cost seems high, it should be noted that the cost here is based on our laboratory data. It is clear that the cost preparation is reduced when we scale up production under laboratory conditions. Therefore, the preparation cost of this adsorbent can be greatly reduced when it is mass-produced in the industry. For instance, reducing the cost of Chitosan-SH preparation from the source in industry is crucial to reduce the production cost of PCSs@chitosan. Therefore, on the basis of the above-mentioned considerations, PCSs@chitosan would have broad prospects of application to new adsorbing agent.

Antibacterial test

Escherichia coli and Staphylococcus aureus were selected as model bacteria to test the antibacterial activity of the adsorbent. Individual bacterial colonies were first isolated and grown in 5 mL of Luria Bertani (LB) broth. All inoculated tubes were incubated at 37 °C for 12 hours and strains were harvested at the logarithmic growth stage. A stock bacterial suspension was obtained at a concentration of 10^9 CFU mL^{-1}. Obtain 0.5 mL of each bacterial suspension (10^8 CFU mL^{-1}) by diluting the colonies and spreading them on the surface of agar plates. All test materials were added to the diluted bacterial solution (2.5 mL) and shaken separately at 37 °C for 90 min. After that, 100 μL of the diluted bacterial suspension was inoculated on agar plates and incubated at 37 °C for 18 hours. Bacterial survival was assessed based on the number of colony-forming units. By using a microplate fluorescence spectrometer (Tecan Spark) to measure the luminescence at 600 nm. Optical Density (OD) was used to measure bacterial growth rate.

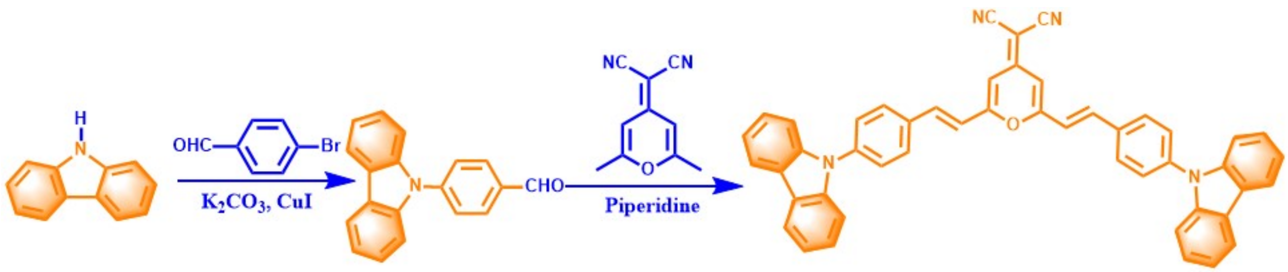

Fig. S1 Synthetic route of CZ-B-DCM.

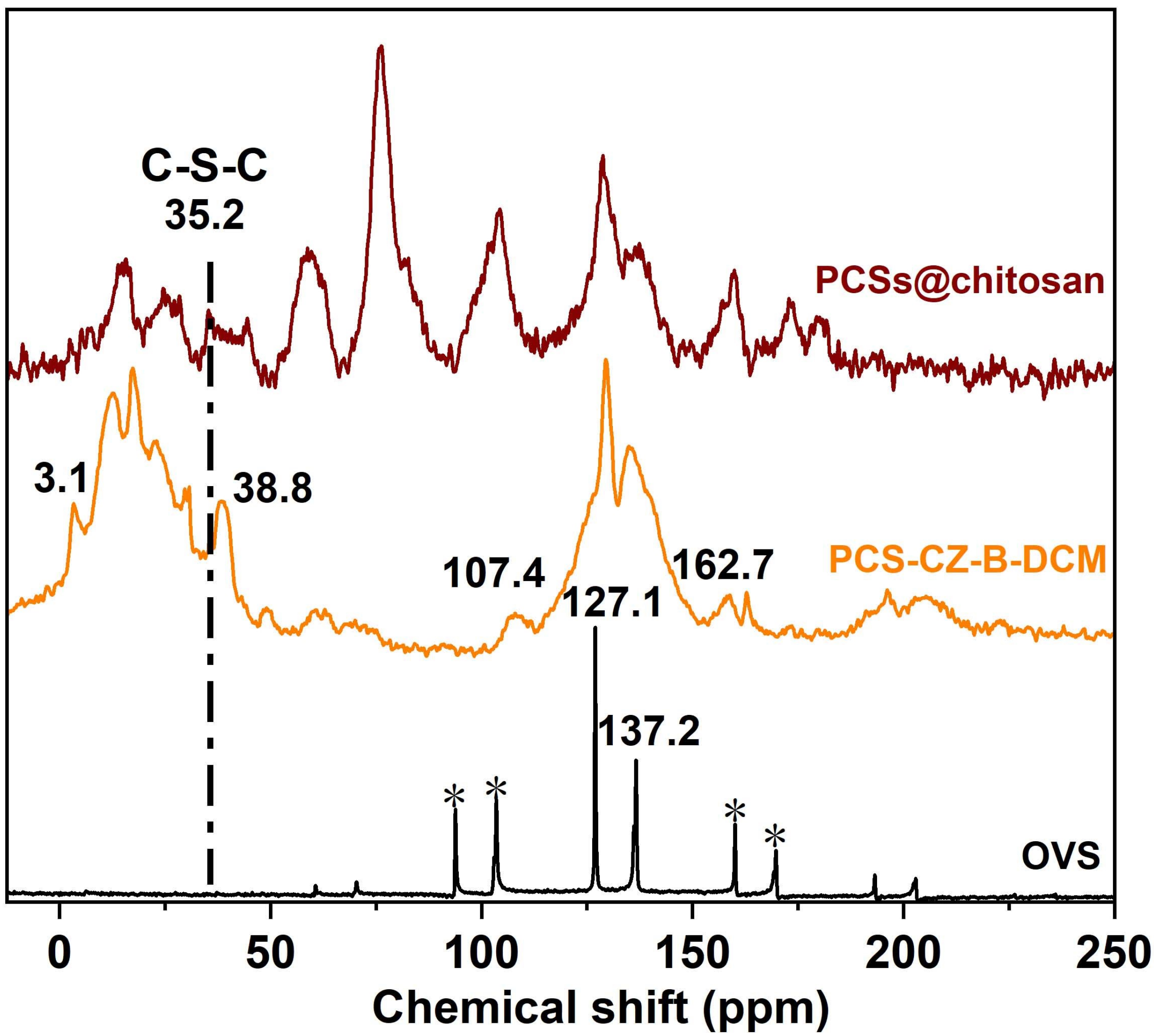

Fig. S2 Solid-state ^{13}C NMR spectra of OVS, PCS-CZ-B-DCM, and PCSs@chitosan. Asterisks denote spinning sidebands.

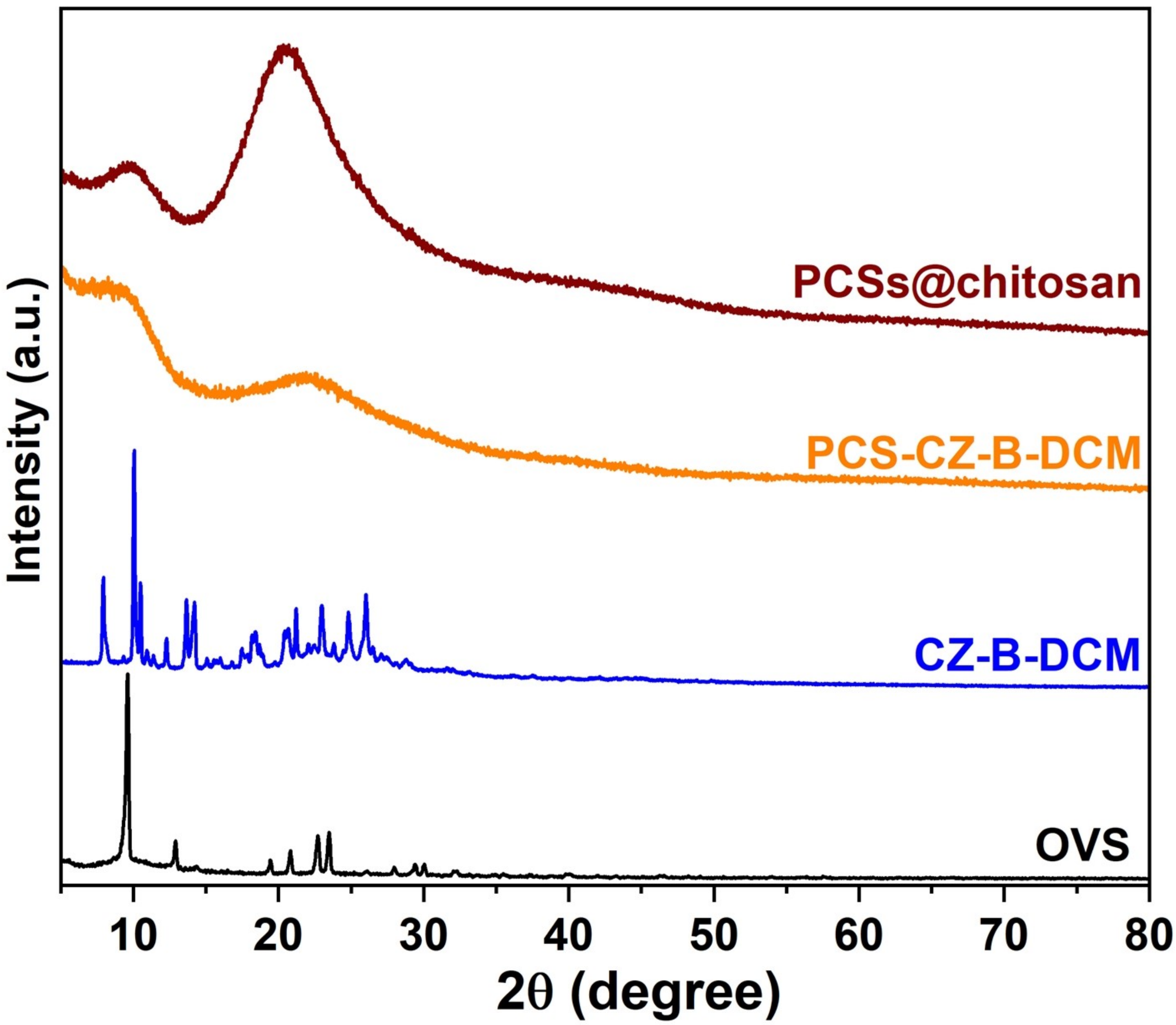

Fig. S3 PXRD patterns of OVS, CZ-B-DCM, PCS-CZ-B-DCM, and PCSs@chitosan.

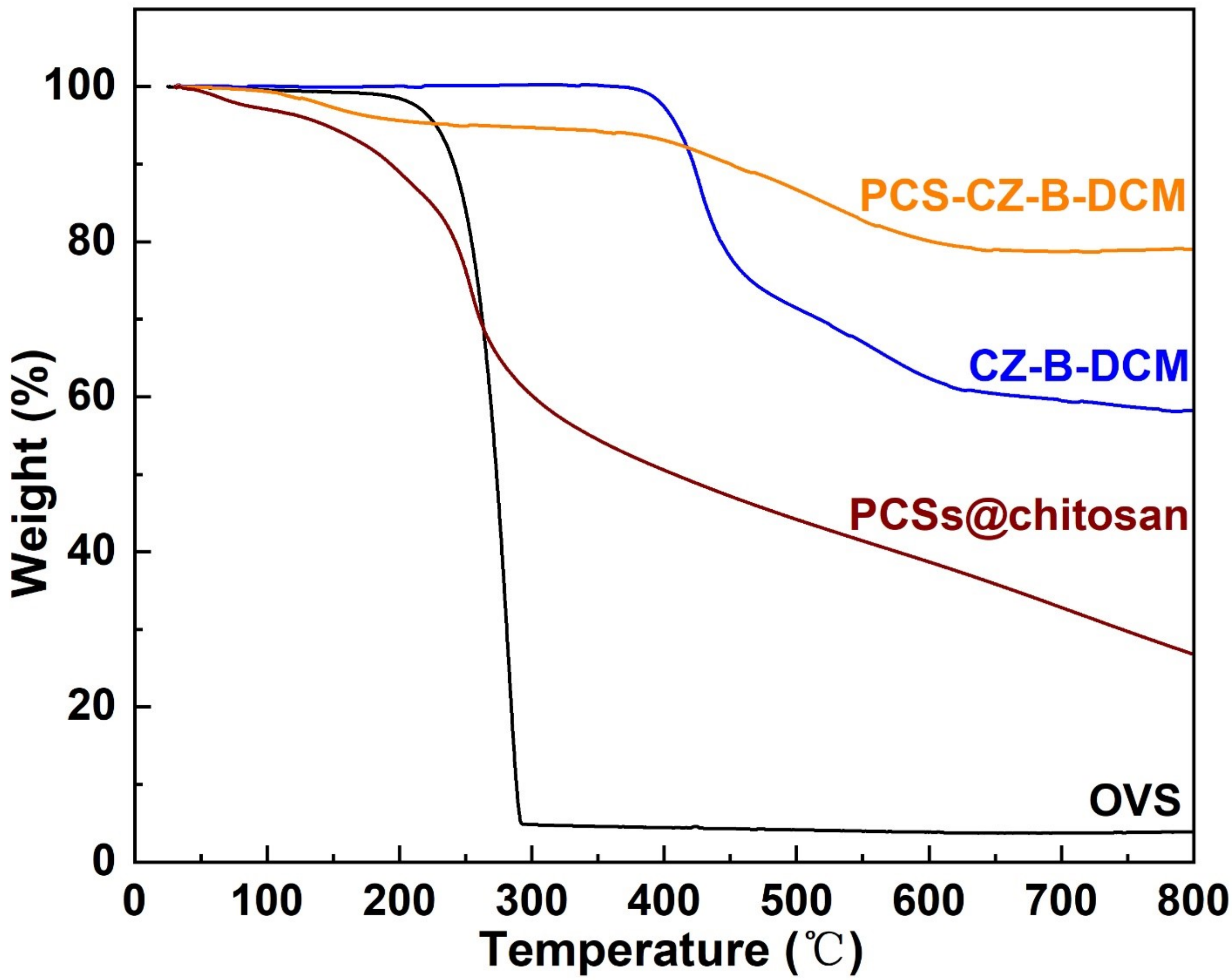

Fig. S4 TGA curves of OVS, CZ-B-DCM, PCS-CZ-B-DCM, and PCSs@chitosan (black, blue, orange, and red present TGA curves of OVS, CZ-B-DCM, PCS-CZ-B-DCM, and PCSs@chitosan, respectively).

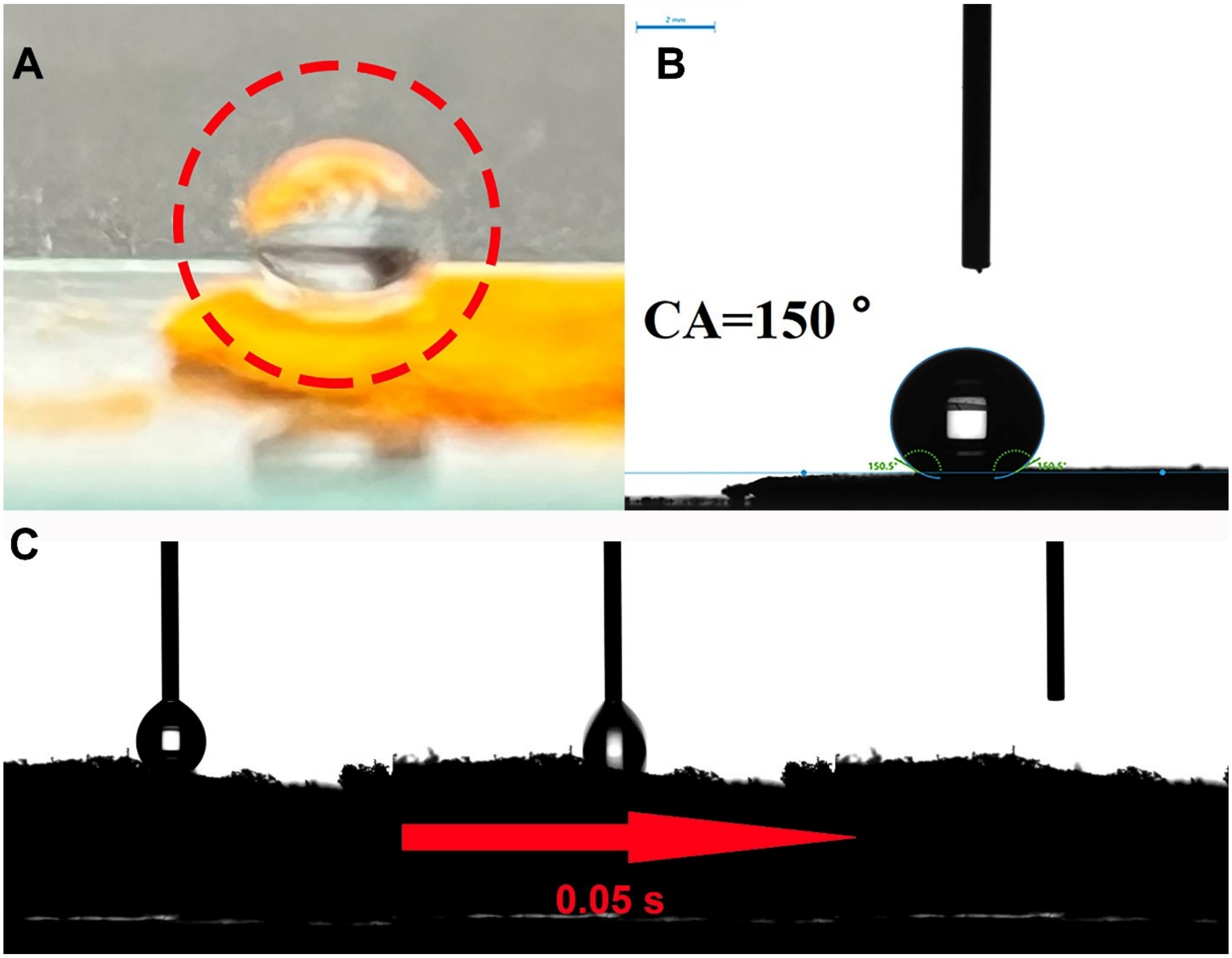

Fig. S5 The superhydrophobic/superhydrophilic properties of PCS-CZ-B-DCM and PCSs@chitosan. (A) Image of droplets on PCS-CZ-B-DCM. (B) Water contact angle (CA) image of PCS-CZ-B-DCM. c Images of a droplet impact on the surfaces of PCSs@chitosan.

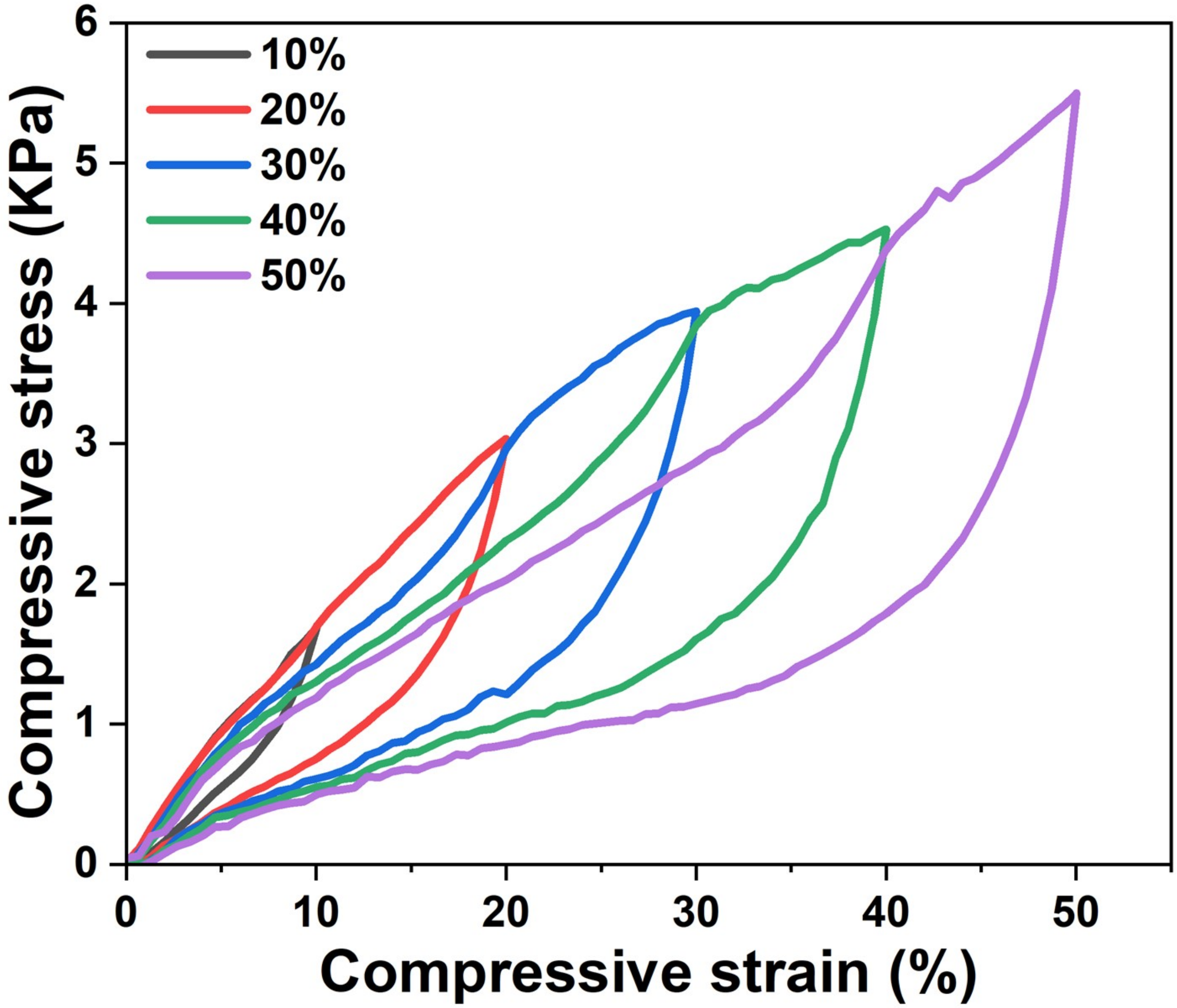

Fig. S6 Stress-strain curves of PCSs@chitosan at 10%, 20%, 30%, 40% and 50% of the maximum strain.

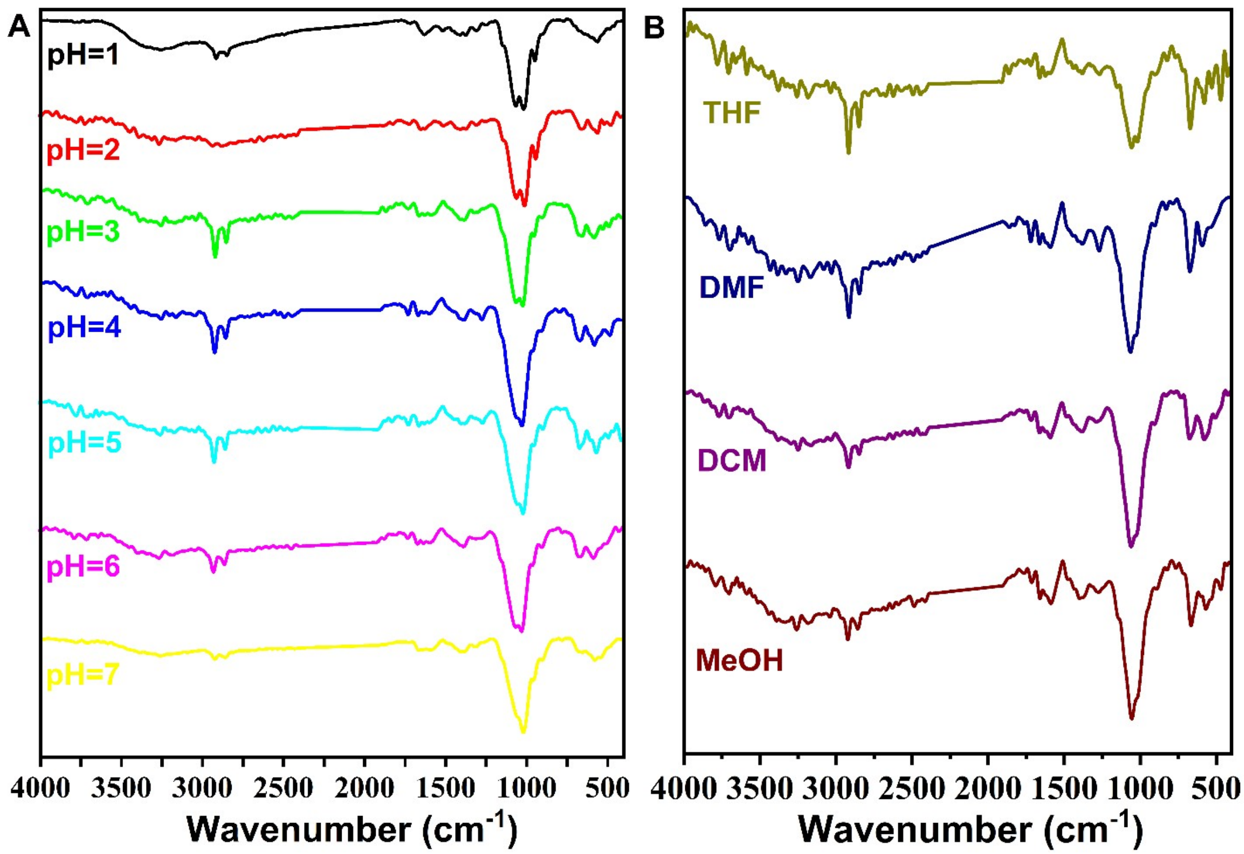

Fig. S7 FT-IR spectra of PCSs@chitosan after treatment in different solvents over 24 h.

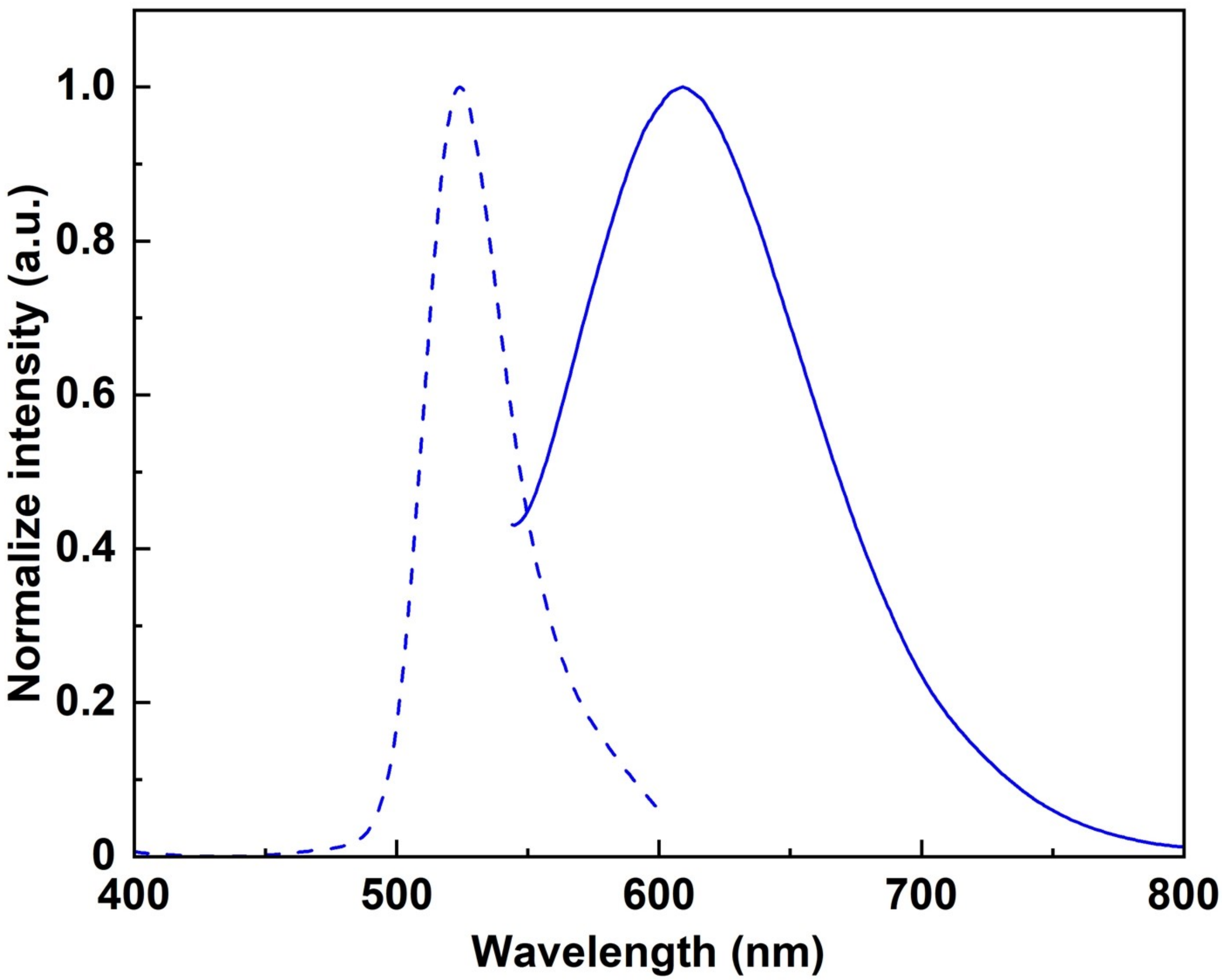

Fig. S8 Normalized excitation emission and fluorescence emission spectra of CZ-B-DCM (dashed and solid lines represent excitation and emission spectra, respectively).

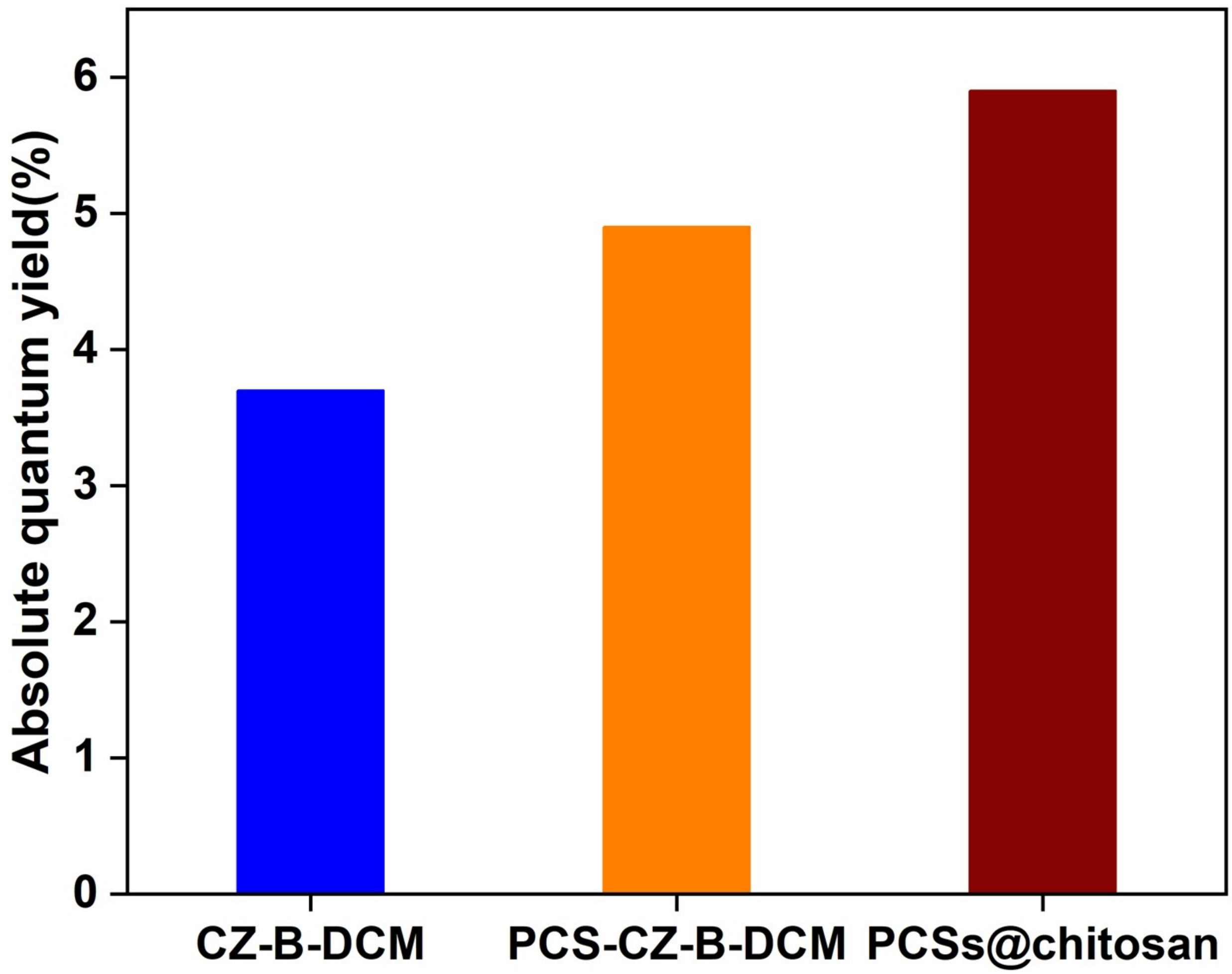

Fig. S9 The absolute quantum yields of CZ-B-DCM, PCS-CZ-B-DCM, and PCSs@chitosan (blue, orange, and red present quantum yield of CZ-B-DCM, PCS-CZ-B-DCM, and PCSs@chitosan, respectively).

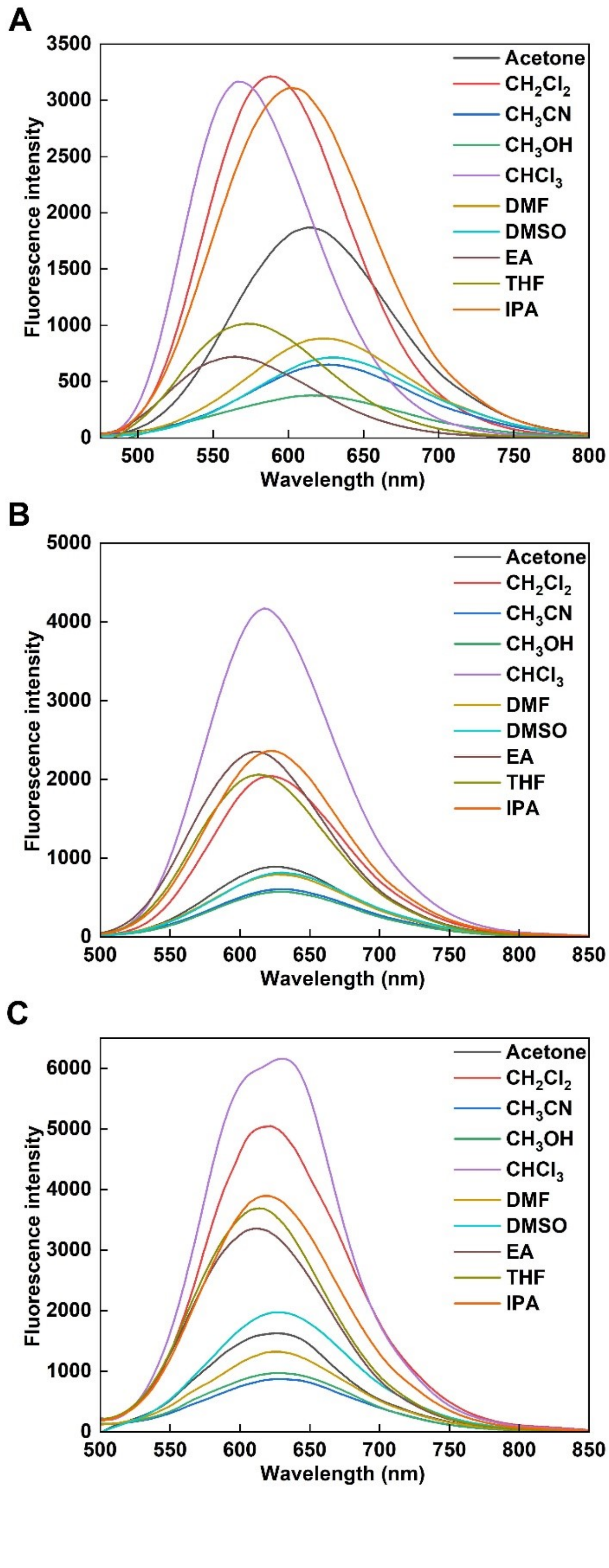

Fig. S10 Effect of different solvents on emission. Emission spectra of (A) CZ-B-DCM (B) PCS-CZ-B-DCM, and (C) PCSs@chitosan.

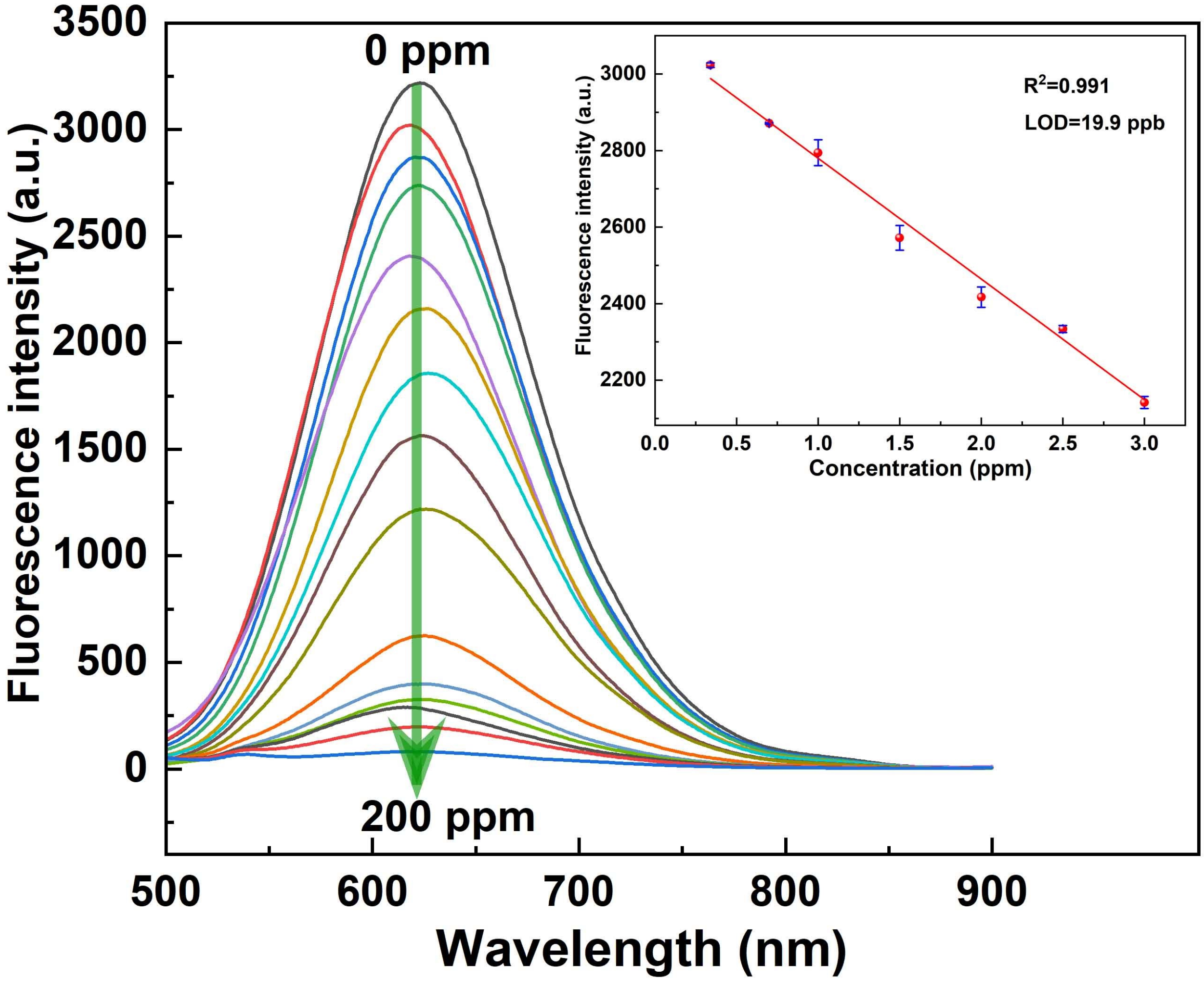

Fig. S11 Fluorescence spectra of PCS-CZ-B-DCM in the presence of an increasing concentration of Au(III) (from 0 to 200 ppm) (inset: profiles of the emission intensity versus Au(III) concentration showing a good linear relationship). The error bars express the standard deviation (n = 3).

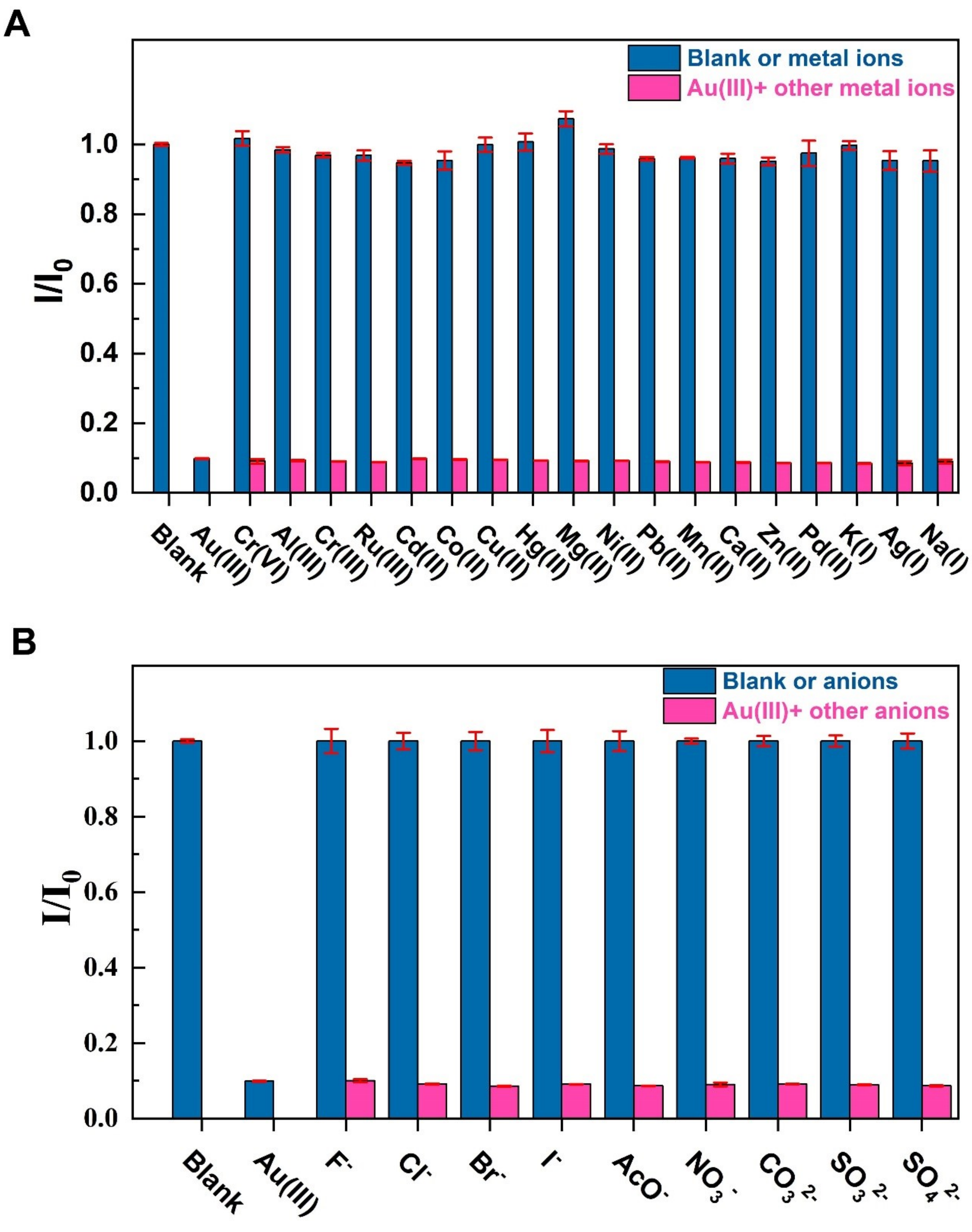

Fig. S12 Selectivity detection. Comparison of the relative emission intensity ratio (I/I_0) indicates indicating a good selectivity for Au(III) detection over (A) 18 metal ions and (B) 9 anions for PCSs@chitosan. The error bar in (A) and (B) represents the standard deviation of three independent measurements.

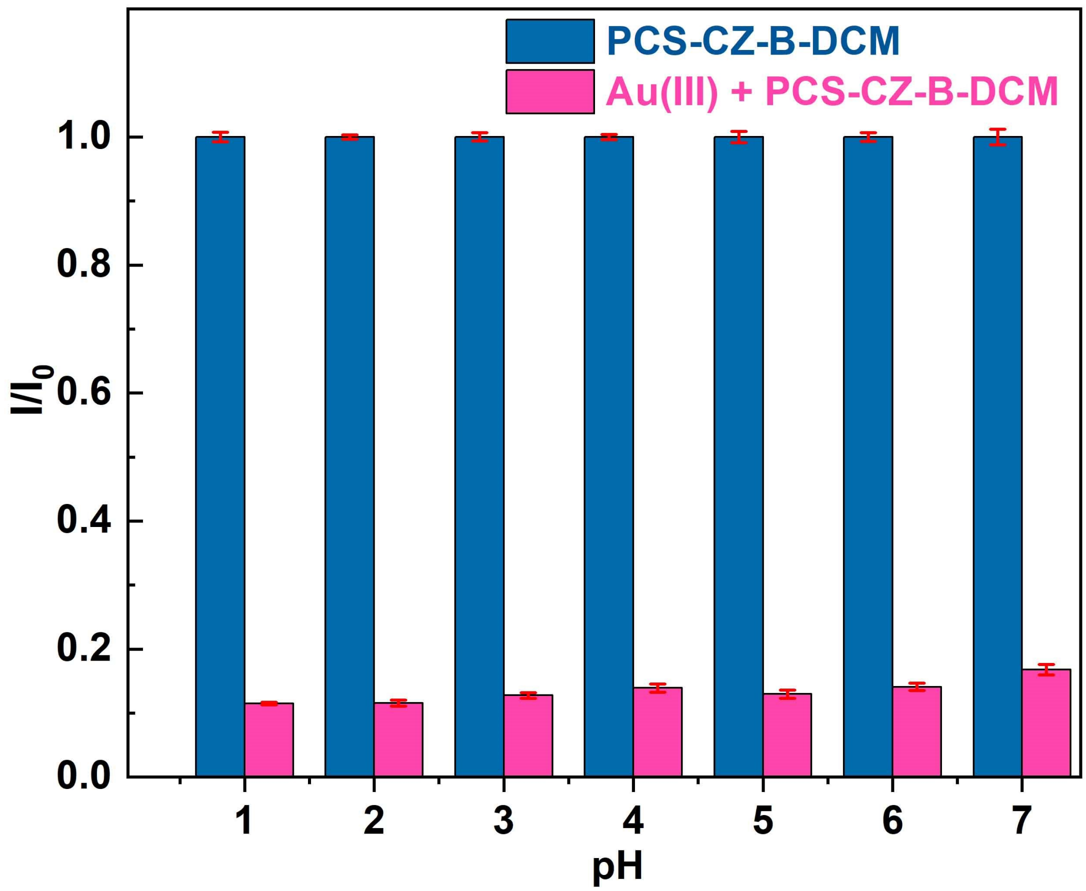

Fig. S13 The effect of different pH on the detection of Au(III) by PCS-CZ-B-DCM. The error bars express the standard deviation (n = 3).

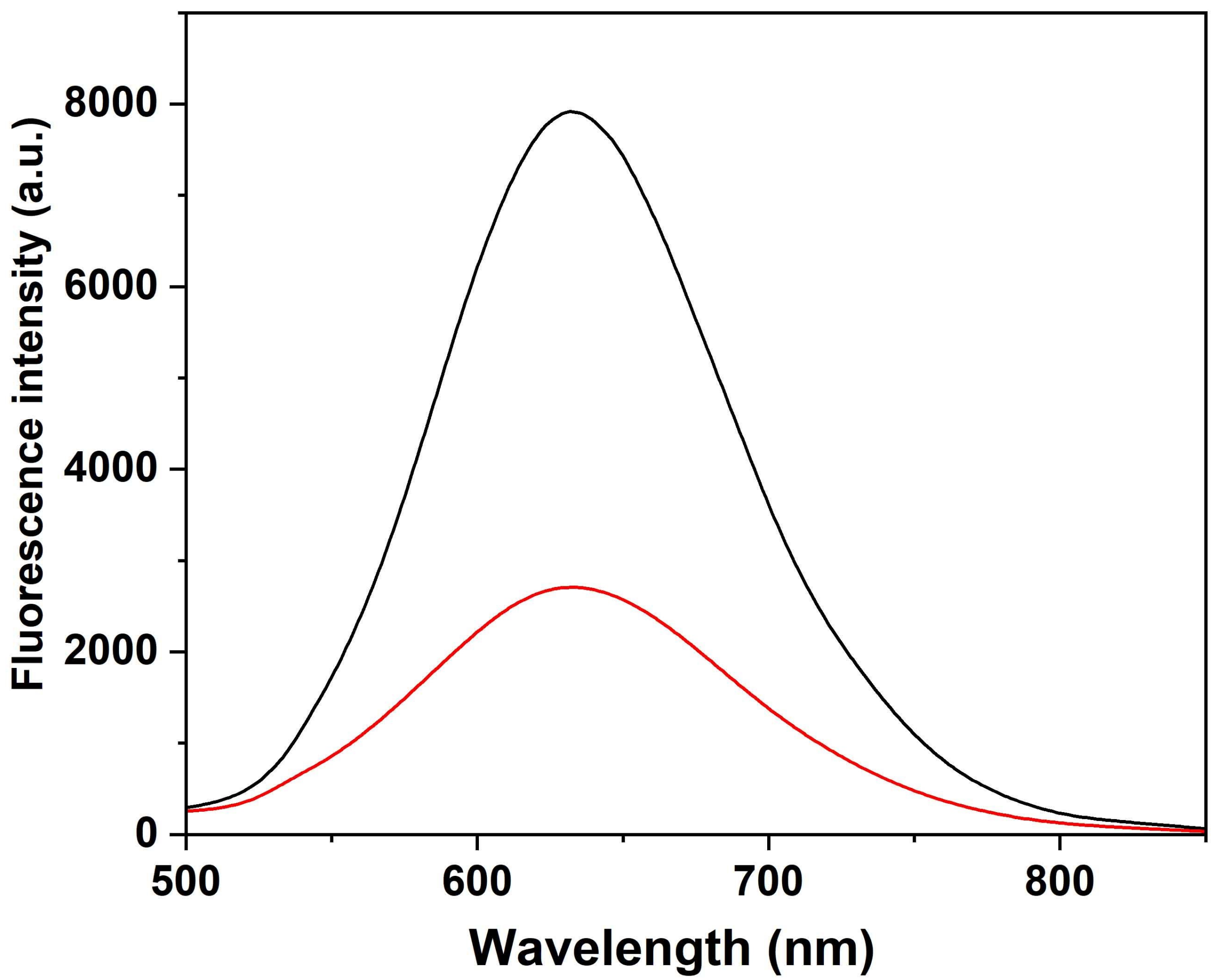

Fig. S14 Detection of gold in industrial plating waste water. The emission spectra (black line) and after immersing into industrial gold plating waste water (red line). The gold plating waste solutions contained gold, copper, and iron with concentration of 10.2, 22.6, and 36.7 ppm.

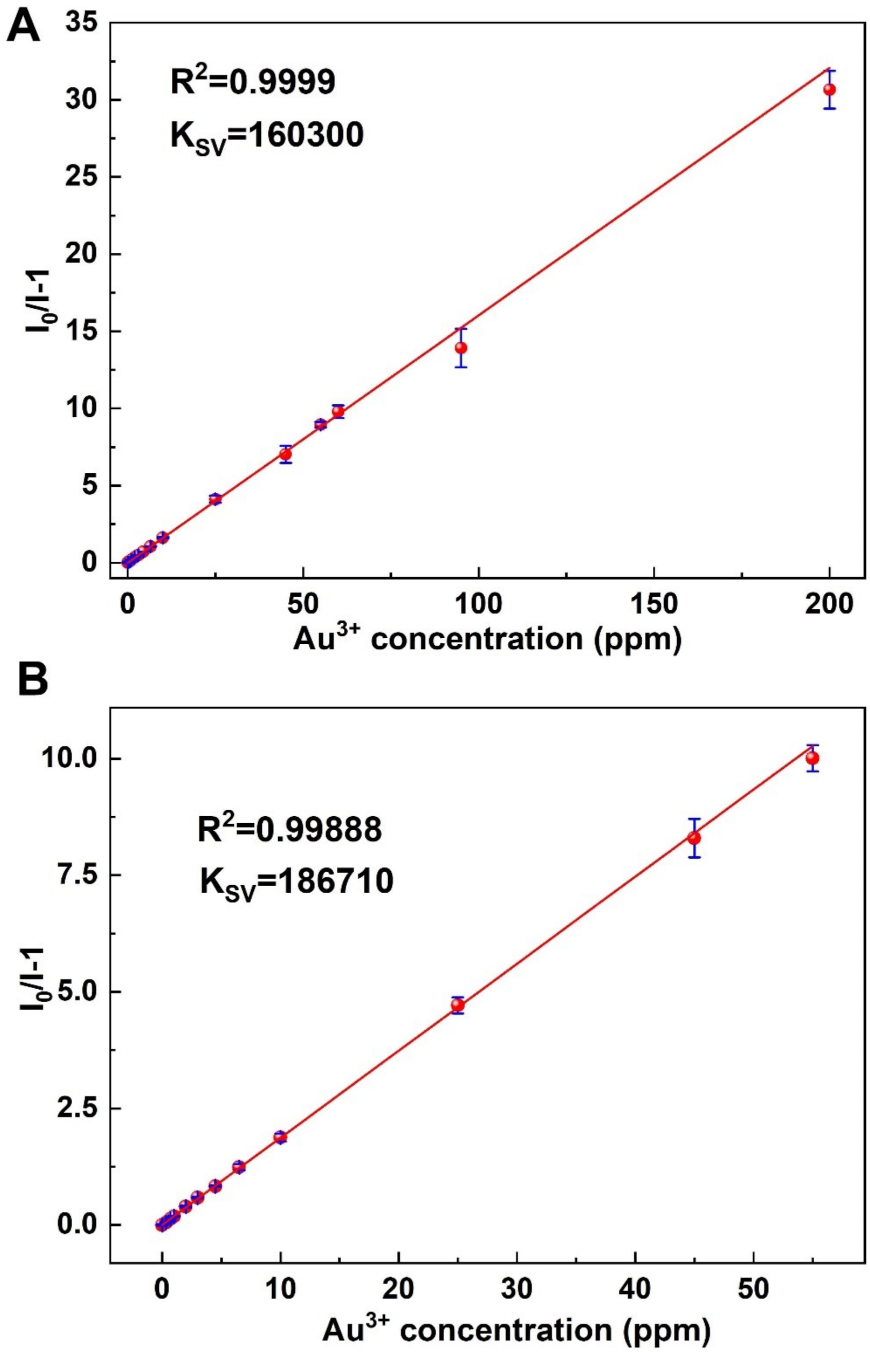

Fig. S15 Determination of K_{SV}. The Stern-Volmer plot for the quenching of (A) PCS-CZ-B-DCM and (B) PCSs@chitosan by Au(III). The error bar represents the standard deviation of three independent measurements.

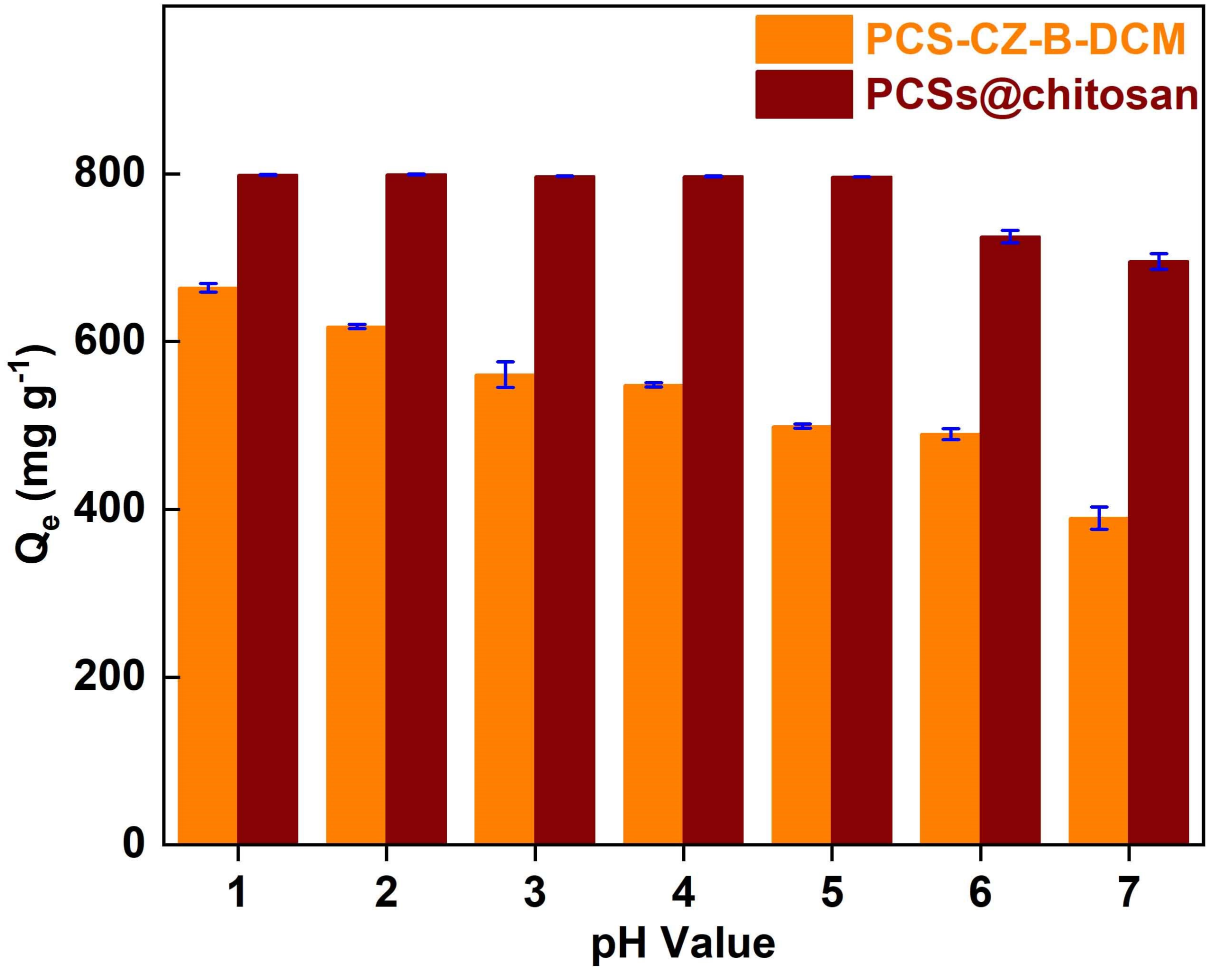

Fig. S16 Effect of pH value on the adsorption of gold on PCS-CZ-B-DCM (orange) and PCSs@chitosan (red) at initial concentration of 200 ppm under visible light irradiation. The error bar represents the standard deviation of three independent measurements.

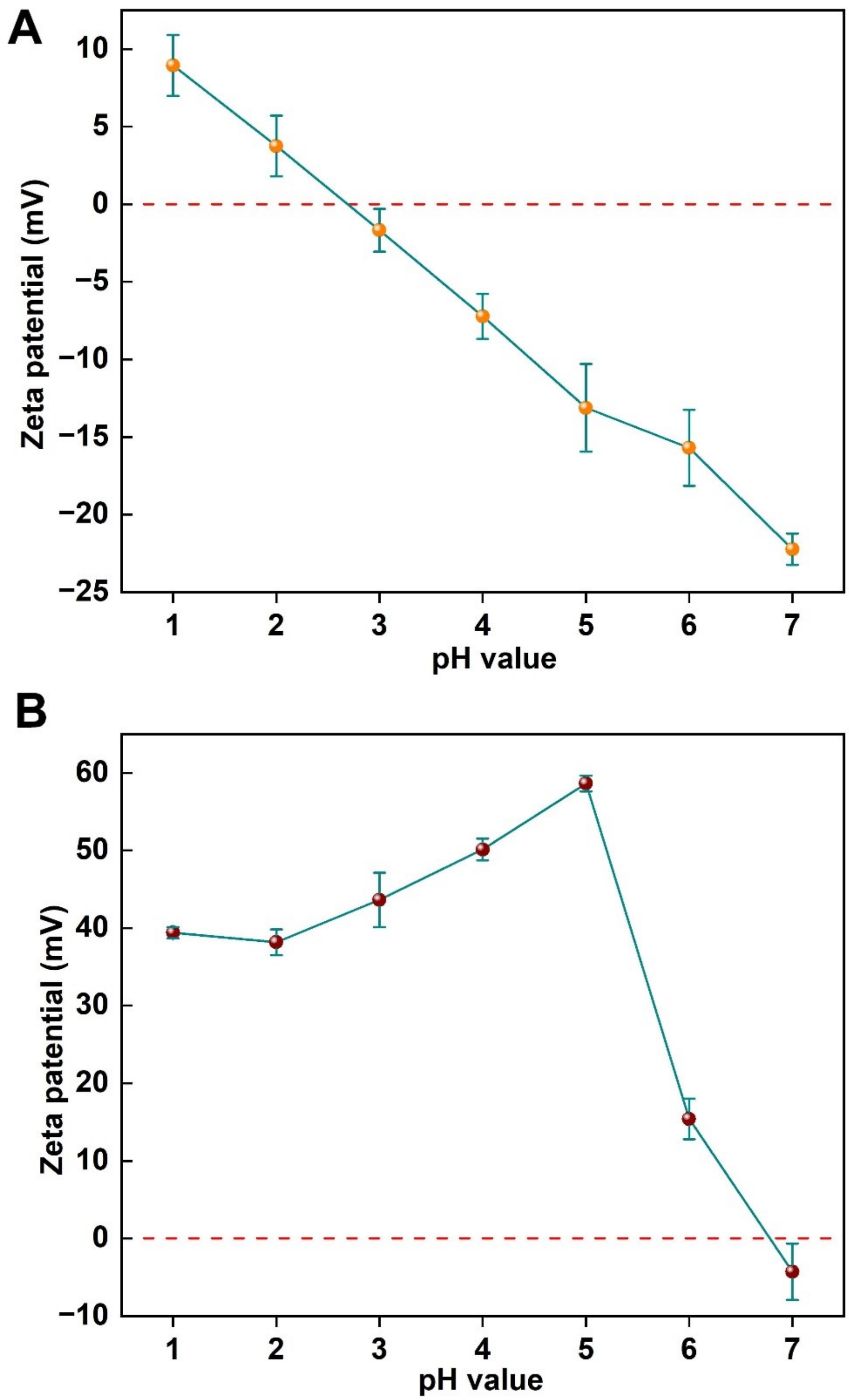

Fig. S17 Zeta potential. The Zeta potential analysis of (A) PCZ-CZ-B-DCM and (B) PCSs@chitosan under different pH values.

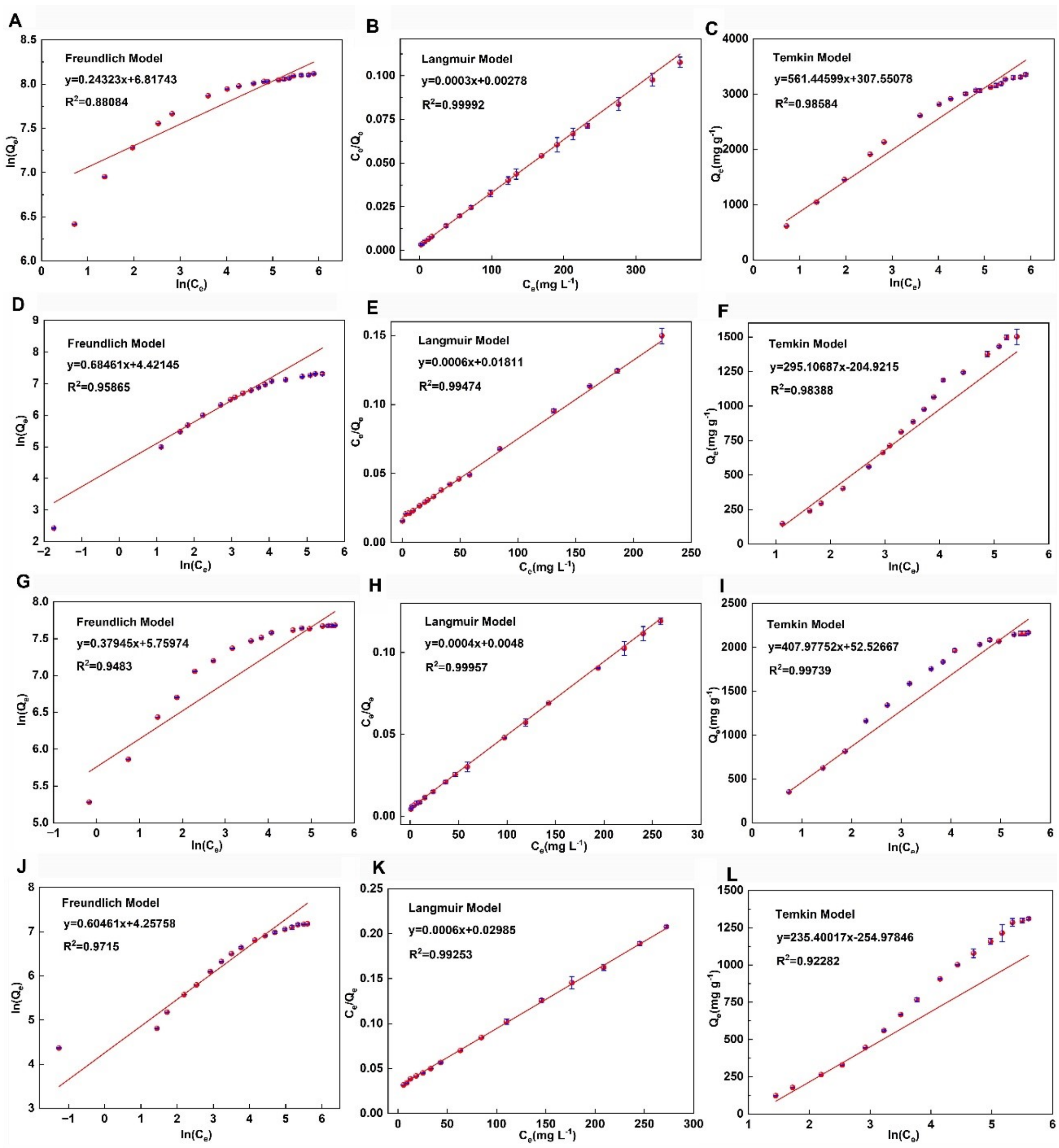

Fig. S18 Adsorption equilibrium isotherm and relevant parameters. The adsorption isotherms of PCSs@chitosan were fitted with the (A) Freundlich, (B) Langmuir and (C) Temkin isotherm models under visible light. The adsorption isotherms of PCSs@chitosan were fitted with the (D) Freundlich, (E) Langmuir and (F) Temkin isotherm models under darkness. The adsorption isotherms of PCS-CZ-B-DCM were fitted with the (G) Freundlich, (H) Langmuir and (I) Temkin isotherm models under visible light. The adsorption isotherms of PC-CZ-B-DCM were fitted with the (J) Freundlich, (K) Langmuir and (L) Temkin isotherm models under darkness. The error bar represents the standard deviation of three independent measurements.

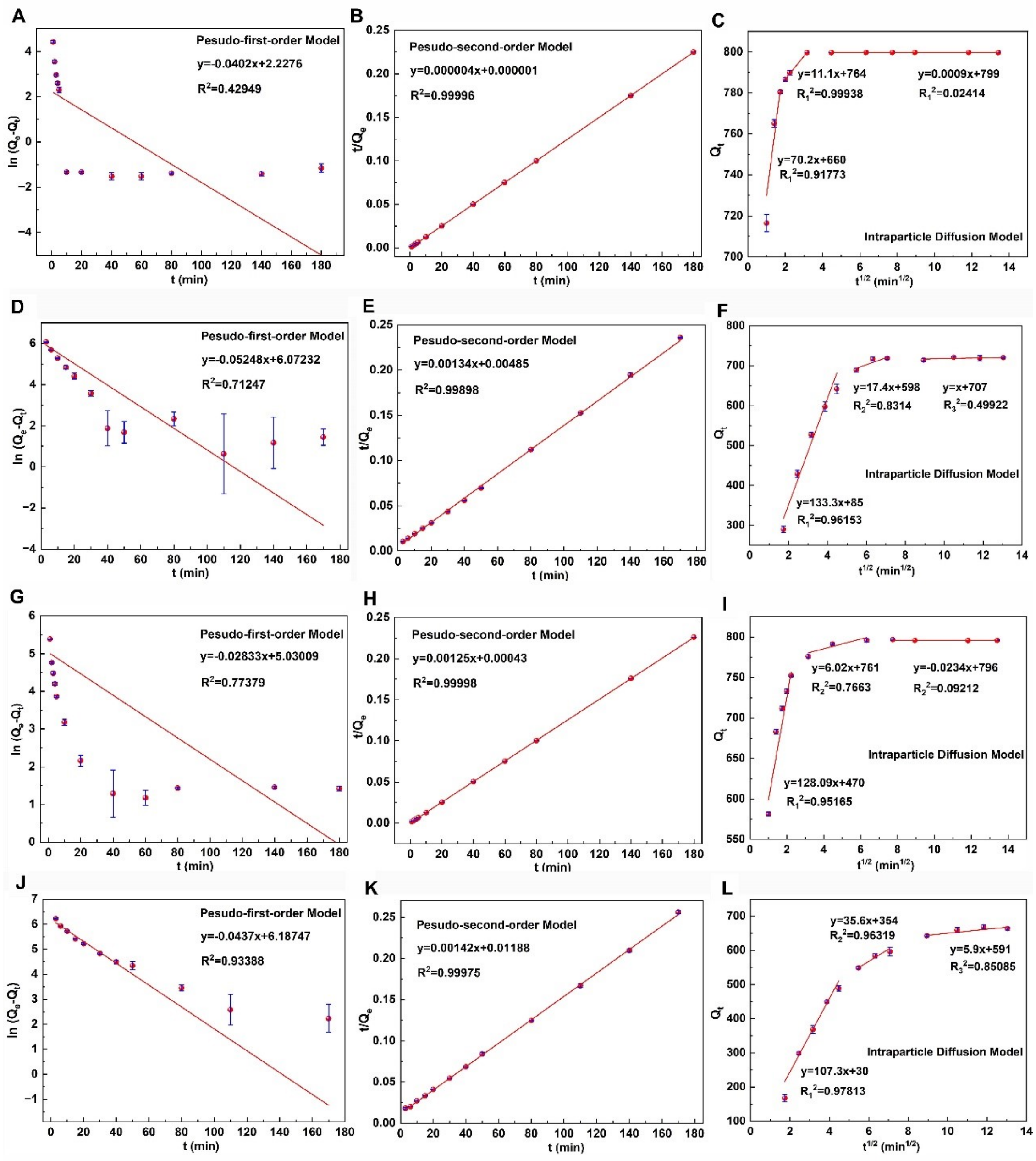

Fig. S19 Adsorption kinetic studies. The (A) pseudo-first-order, (B) pseudo-second-order, and (C) intraparticle diffusion kinetic model plots under visible light for Au (III) by PCSs@chitosan. The (D) pseudo-first-order, (E) pseudo-second-order, and (F) intraparticle diffusion kinetic model plots under darkness for Au (III) by PCSs@chitosan. The (G) pseudo-first-order, (H) pseudo-second-order, and (I) intraparticle diffusion kinetic model plots under visible light for Au (III) by PCS-CZ-B-DCM. The (J) pseudo-first-order, (K) pseudo-second-order, and (L) intraparticle diffusion kinetic model plots under darkness for Au (III) by PCS-CZ-B-DCM. The error bar represents the standard deviation of three independent measurements.

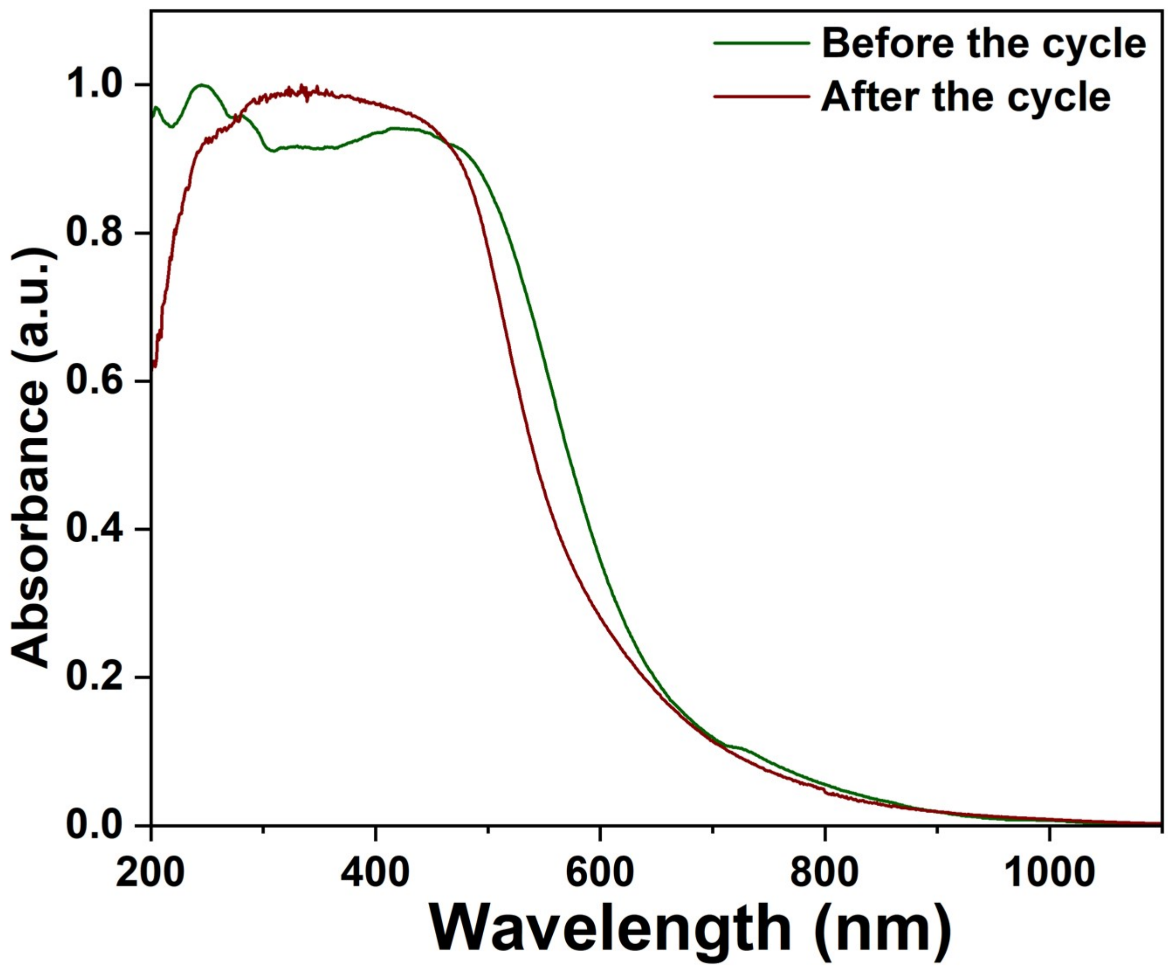

Fig. S20 UV-vis absorption spectra of reused PCSs@chitosan aerogel device after 10 cycles.

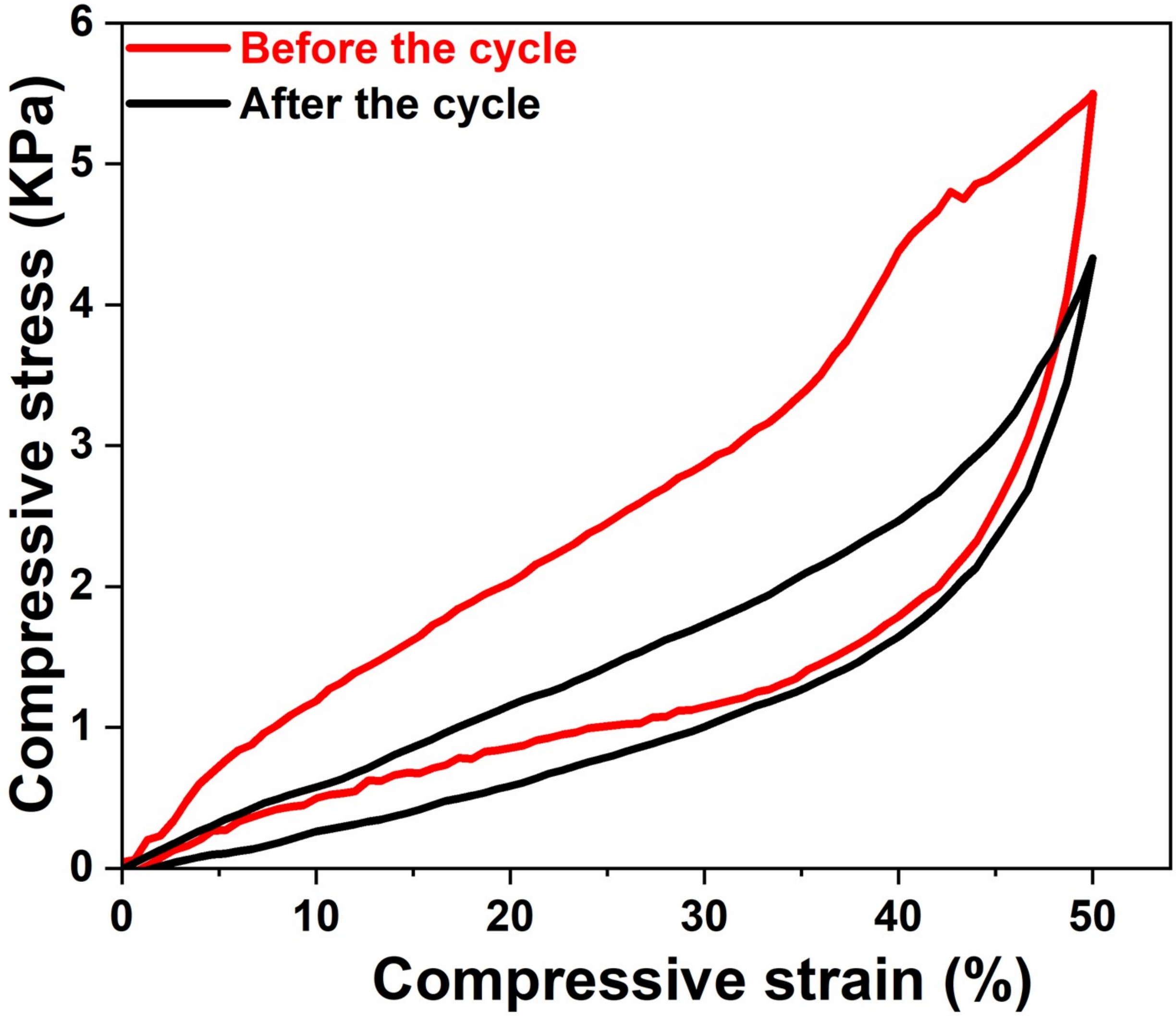

Fig. S21 Stress-strain curves of reused PCSs@chitosan (after using 10 cycles) at 50% strain.

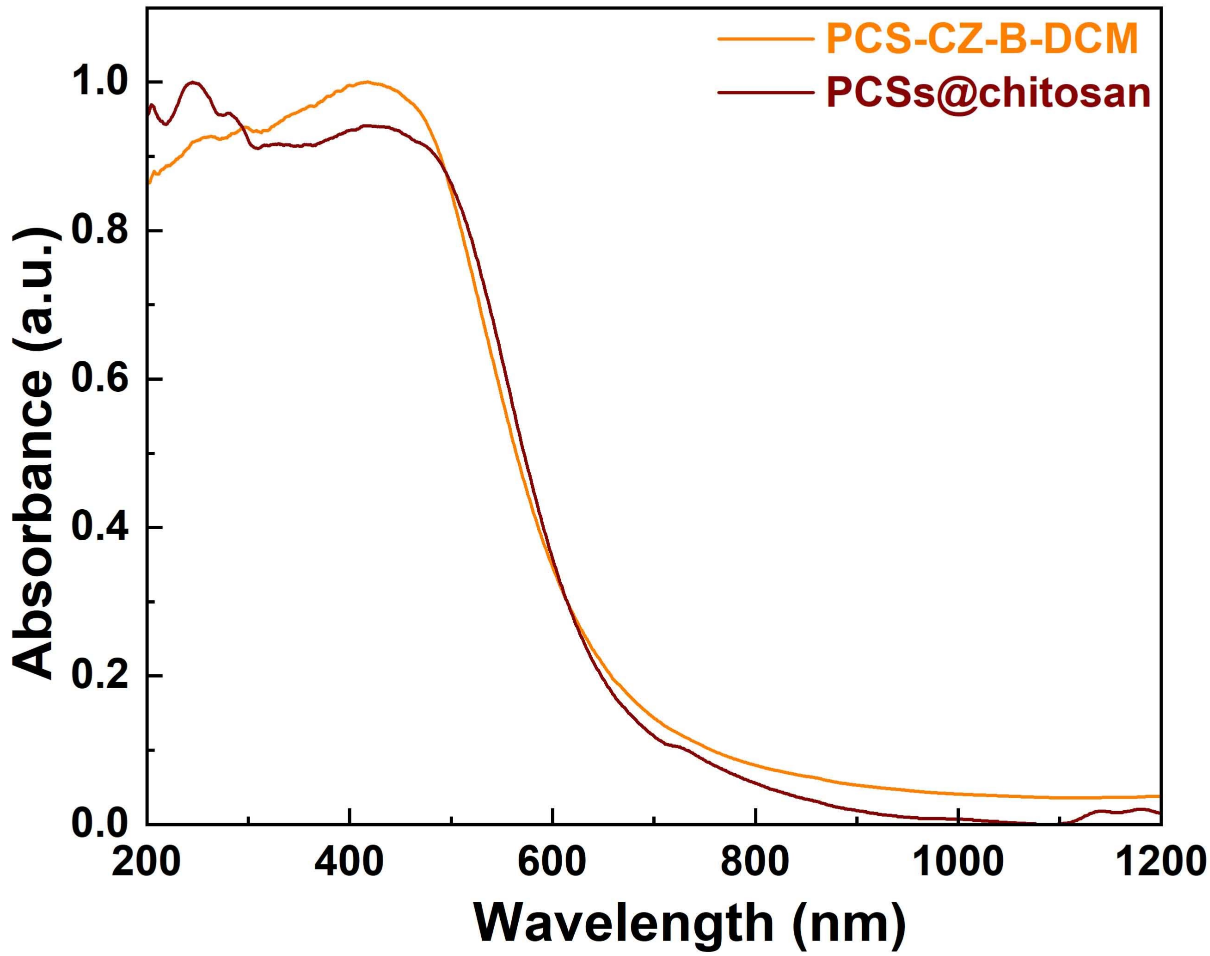

Fig. S22 The UV-vis diffuse reflectance spectra of PCS-CZ-B-DCM and PCSs@chitosan.

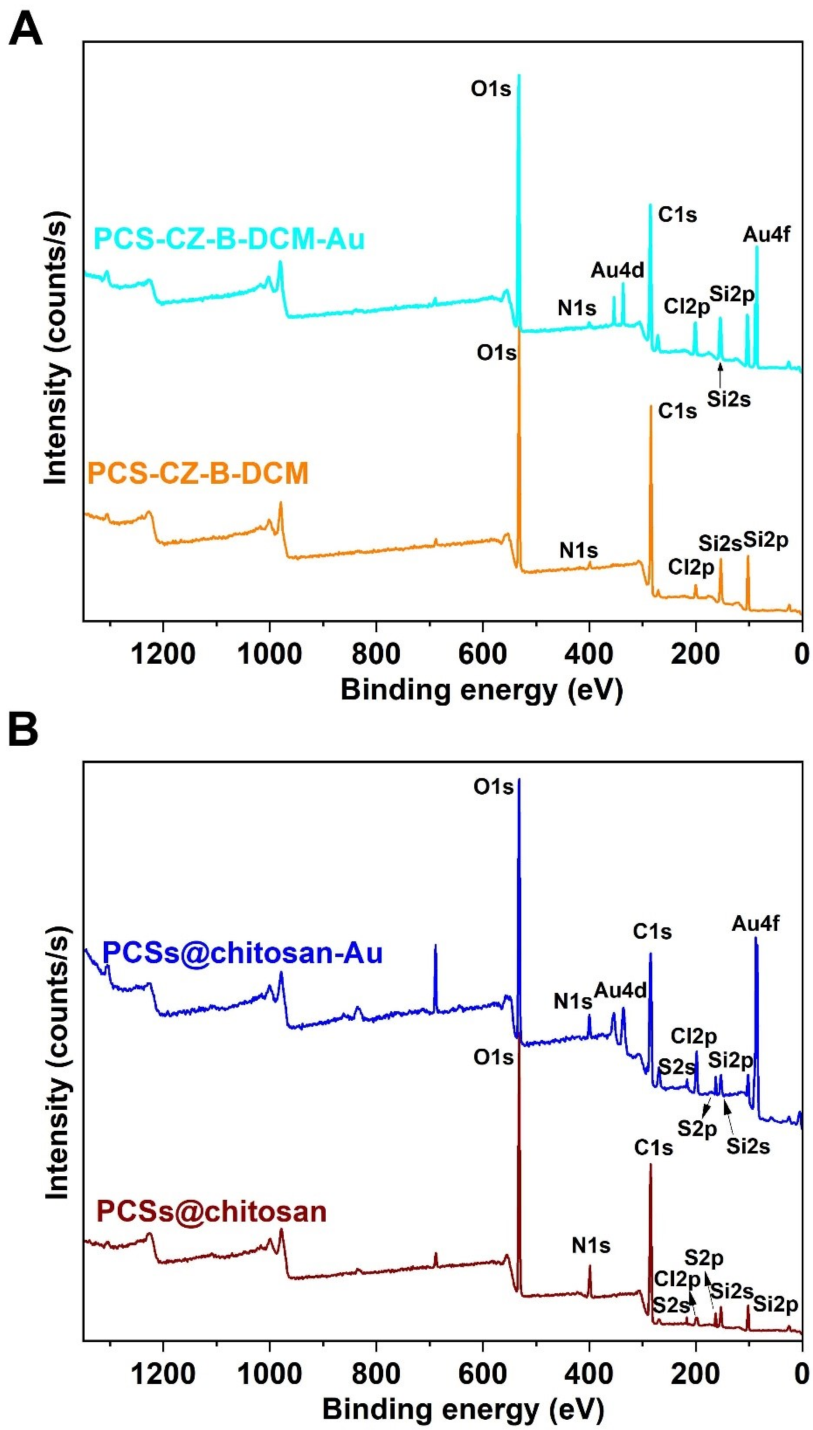

Fig. S23 XPS spectra. XPS survey scan of (A) PCS-CZ-B-DCM and (B) PCSs@chitosan before and after Au (III) adsorption.

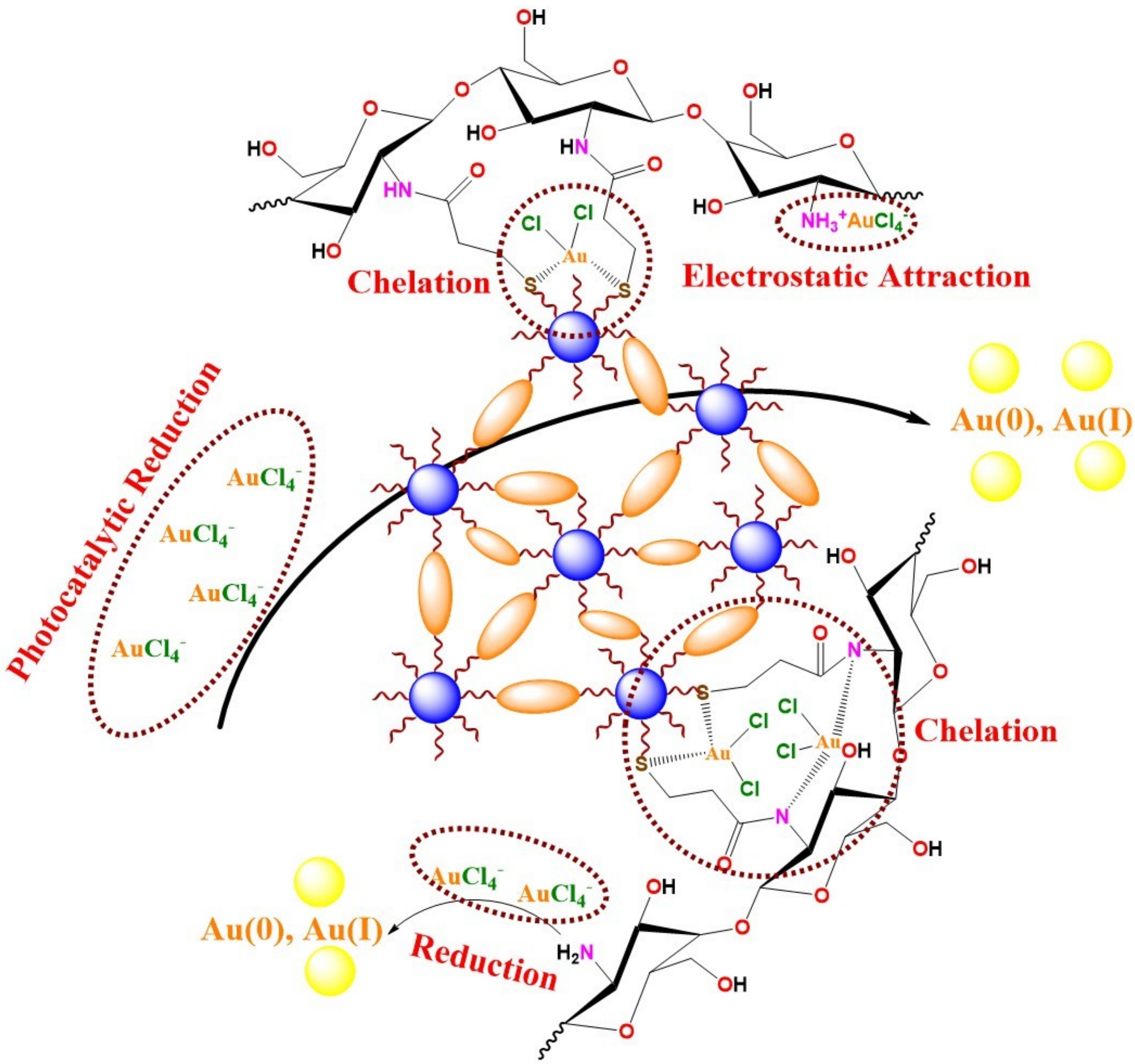

Fig. S24 The mechanism of PCSs@chitosan adsorption of Au(III).

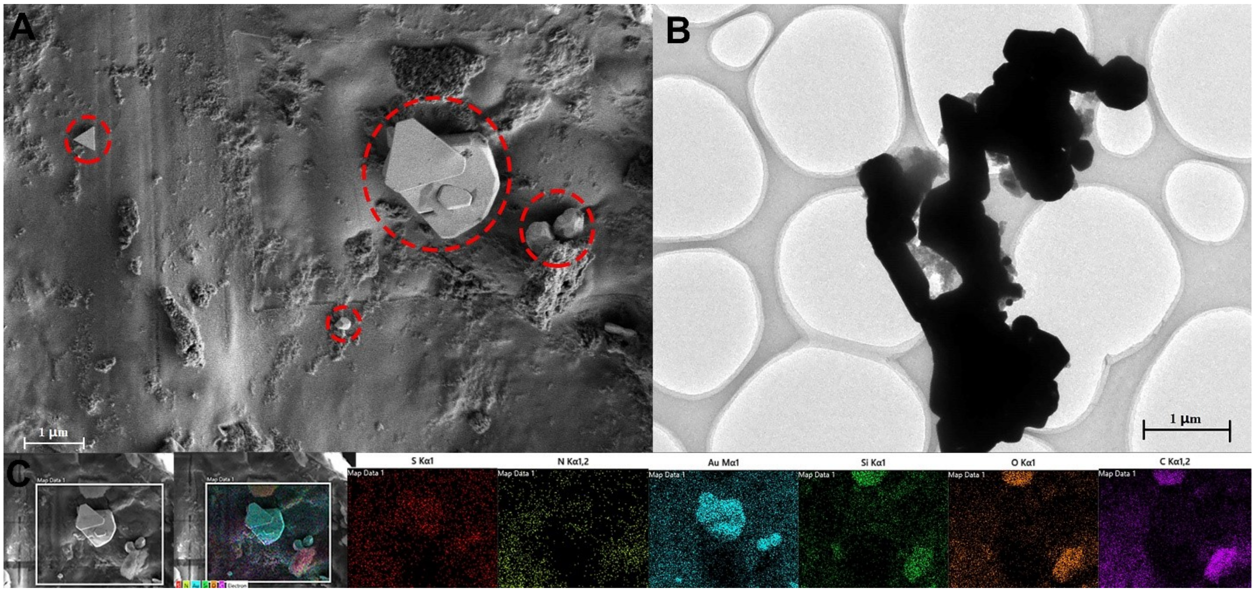

Fig. S25 Characterizations of PCSs@chitosan-Au. (A) FE-SEM images of PCSs@chitosan-Au. (B) HR-TEM images of PCSs@chitosan-Au. (C) SEM−EDS images of PCSs@chitosan-Au.

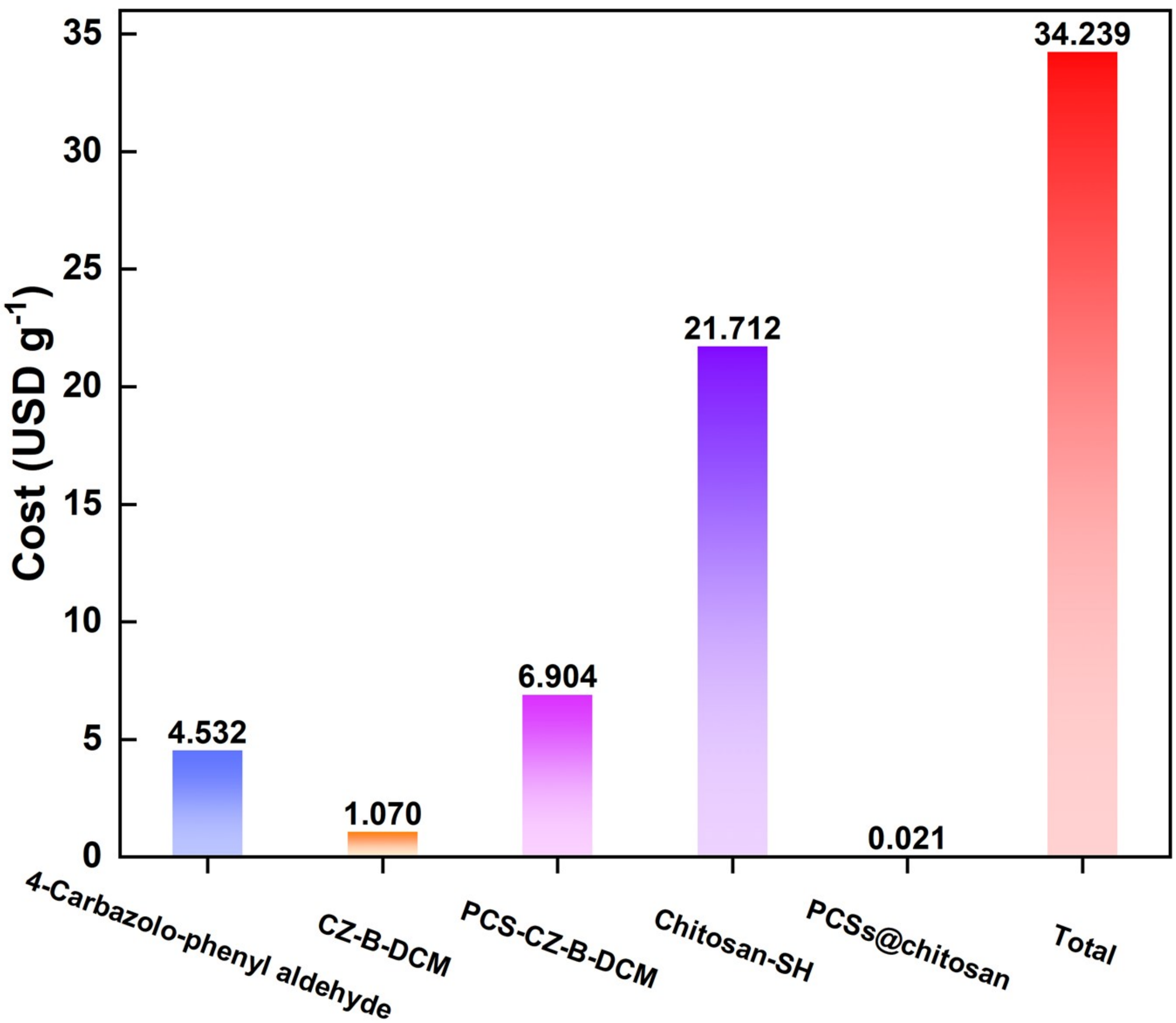

Fig. S26 Production cost distribution of raw materials, electricity in each step for the synthesis of 1 g PCSs@chitosan (small dose feeding, data based on our current research).

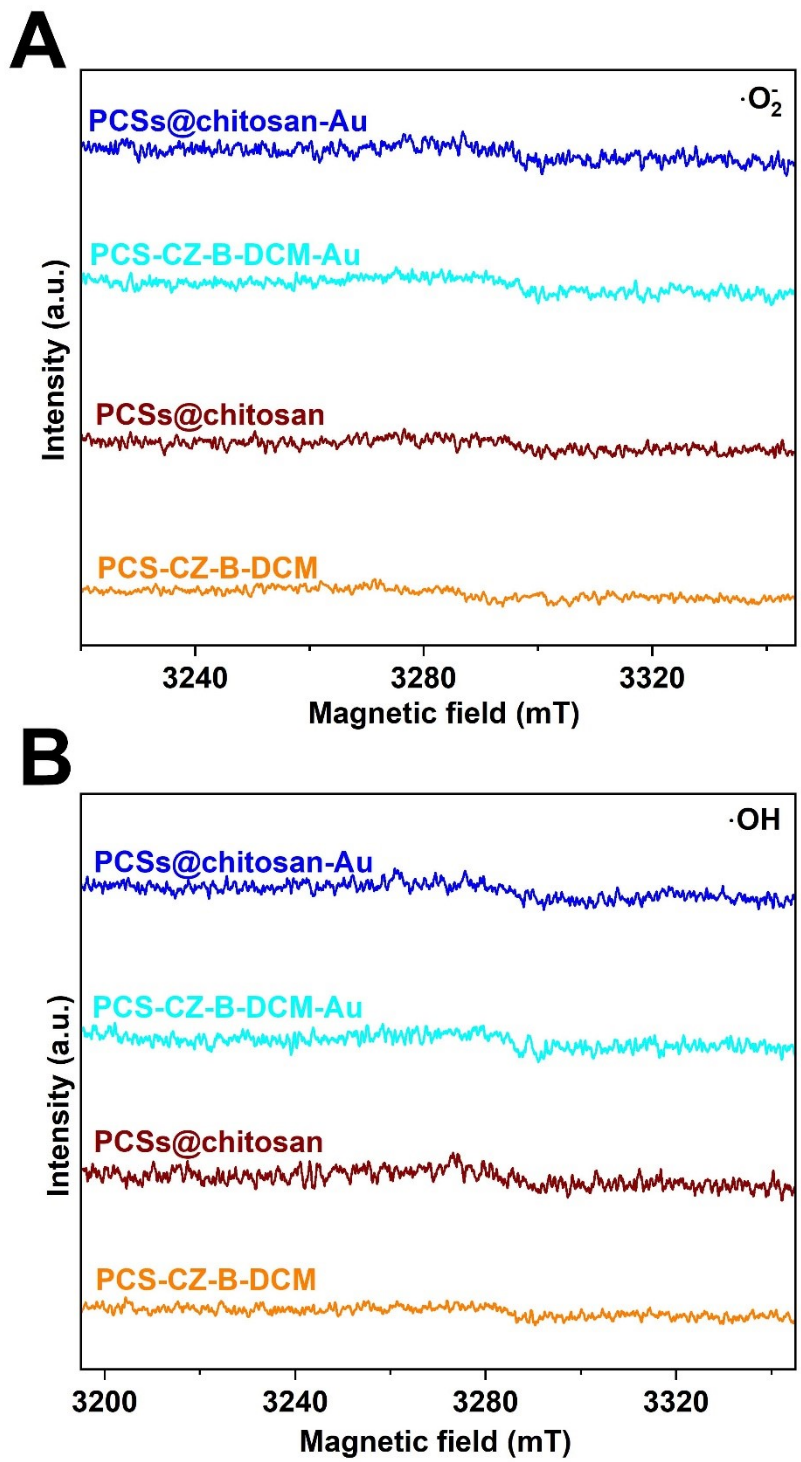

Fig. S27 ESR spectra. ESR spectra of (A) $•O_2^-$ and (B) •OH recorded with the PCS-CZ-B-DCM, PCSs@chitosan, PCS-CZ-B-DCM-Au, and PCSs@chitosan-Au under the dark.

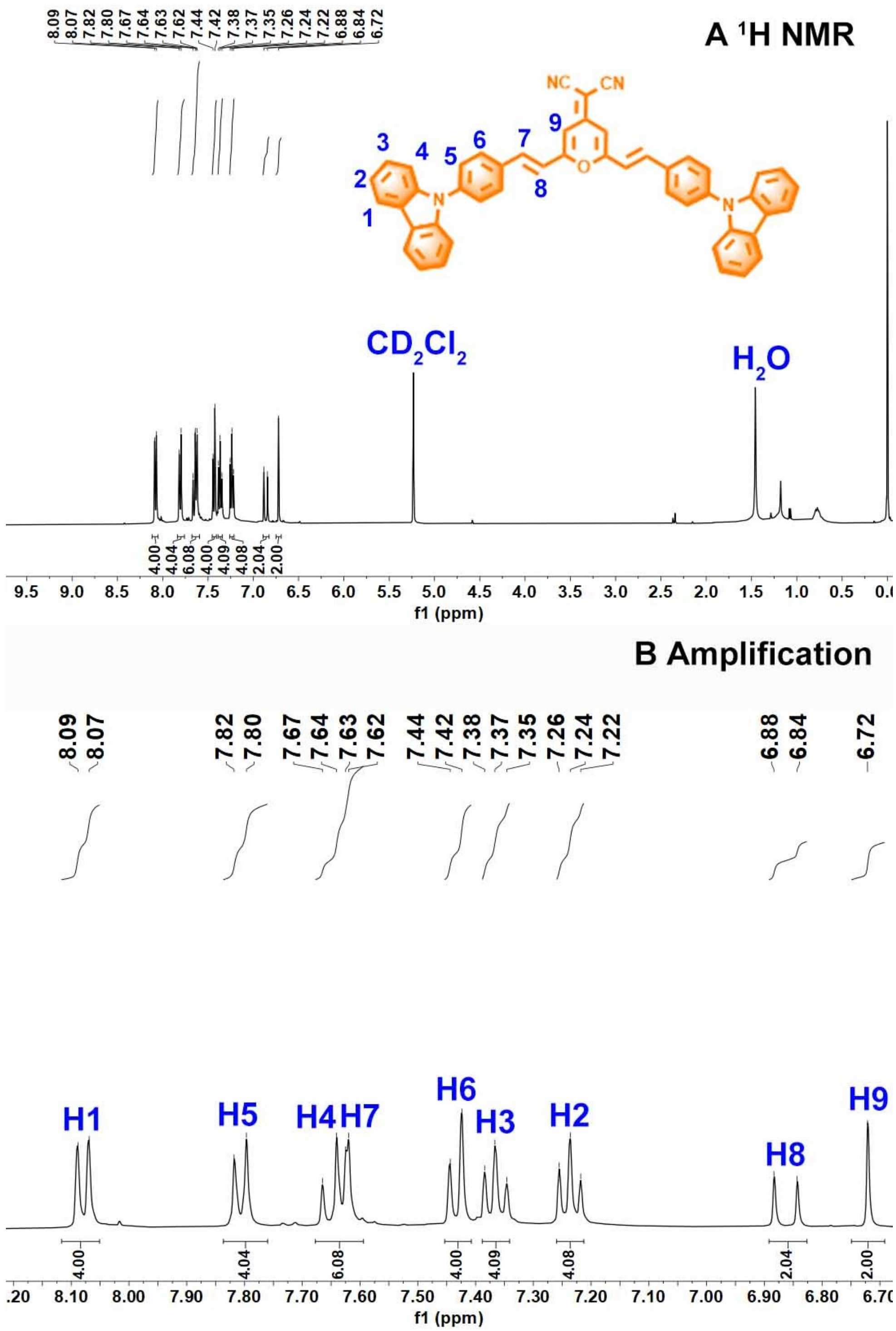

Fig. S28 ^{1}H NMR spectrum of CZ-B-DCM (400 MHz, CD_2Cl_2).

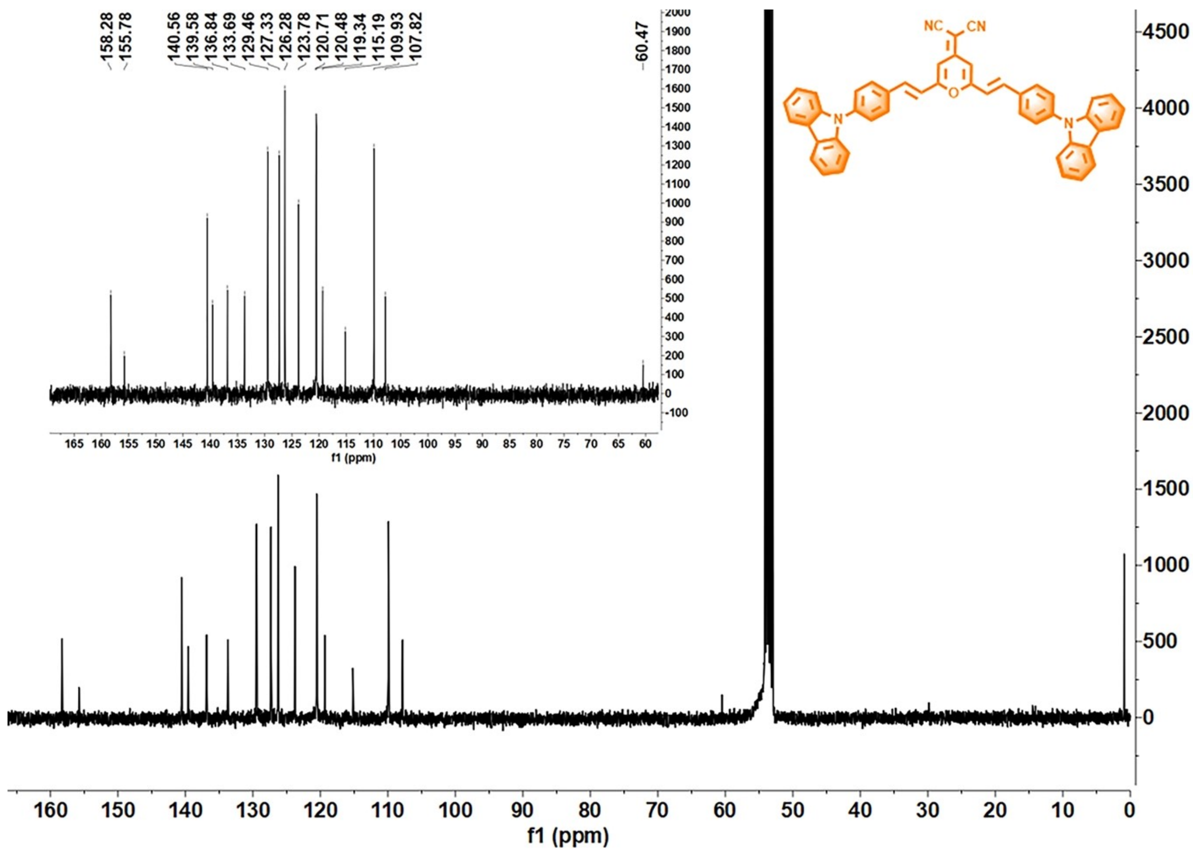

Fig. S29 ^{13}C NMR spectrum of CZ-B-DCM (100 MHz, CD_2Cl_2).

Table S1. Elemental analysis of PCS-CZ-B-DCM.

Sample	Experimental Value			Theoretical Value		
	C%	H%	N%	C%	H%	N%
PCS-CZ-B-DCM	42.3	4.5	1.8	40.0	3.9	1.7

Table S2. Porosity data of PCS-CZ-B-DCM.

S_{BET}[a] /m^2 g^{-1}	S_{micro}[b] /m^2 g^{-1}	V_{total}[c] /cm^3 g^{-1}	$V_{micro\ l}$[d] /cm^3 g^{-1}	V_{micro} /V_{total}
1168.280	301.348	1.343	0.143	0.106

[a] Surface area calculated from the N_2 isotherm.

[b] Microporous surface area calculated from the N_2 adsorption isotherm using the t-plot method.

[c] Total pore volume calculated at $P/P_0 = 0.99$.

[d] The micropore volume derived using the t-plot method.

Table S3. Atomic coordinates for PCS-CZ-B-DCM.

Atom	x (Å)	y (Å)	z (Å)
Si	-16.374631	-6.173635	1.664934
Si	-14.388548	-5.920302	4.273006
Si	-14.933458	-9.014329	0.863669
Si	-14.208429	-4.559542	-0.153985
Si	-12.973593	-8.749114	3.467616
Si	-12.198592	-4.304848	2.445233
Si	-12.746419	-7.388529	-0.954006
Si	-10.774835	-7.11721	1.630547
O	-16.016377	-7.758016	1.190502
O	-15.639352	-5.10803	0.573577
O	-15.691449	-5.944116	3.194555
O	-13.85976	-8.498839	-0.340465
O	-13.492532	-5.871243	-0.953045
O	-13.731007	-7.481017	4.292227
O	-13.166334	-4.075983	1.083116
O	-14.047476	-9.291126	2.277691
O	-13.215904	-4.85592	3.679937
O	-11.604536	-8.131251	2.690808
O	-11.395484	-7.339165	0.069682
O	-11.059829	-5.518946	2.112376
C	-18.214913	-5.877808	1.695148
C	-14.924719	-5.388506	5.976715
C	-15.822933	-10.552338	0.301743
C	-14.619313	-3.161979	-1.353355
C	-12.224874	-7.84961	-2.68485
C	-12.487715	-10.122497	4.629105
C	-8.946606	-7.492571	1.67164
C	-18.811113	-4.939498	0.946075
C	-13.565891	-2.909981	-2.465361
C	-14.392579	-4.329232	6.602975
C	-15.571076	-11.145965	-0.87358
C	-10.947678	-8.02726	-3.051713
C	-11.224733	-10.55595	4.748999
C	-8.269917	-8.013065	0.63724
C	-11.325792	-2.730951	2.929795
C	-10.021966	-2.679489	3.237719
C	-1.226894	-6.459944	1.106975
C	-1.269224	-5.1354	0.77424
O	-0.080895	-4.414599	0.623336
C	1.15592	-5.036221	0.818785
C	1.211507	-6.358557	1.156235
C	0.018604	-7.144902	1.319003

C	0.067443	-8.504939	1.662231
C	-2.420339	-4.293424	0.531961
C	2.240649	-4.099972	0.613793
C	3.558557	-4.385476	0.751588
C	4.678167	-3.469885	0.555725
C	-3.712723	-4.681828	0.66722
C	-4.902595	-3.873856	0.428441
C	4.523204	-2.116026	0.180146
C	5.625352	-1.284924	0.014237
C	6.929442	-1.78232	0.20577
C	7.101501	-3.127427	0.574261
C	5.991813	-3.950179	0.7511
C	-6.171363	-4.436462	0.691382
C	-7.345423	-3.714185	0.497864
C	-7.287002	-2.395417	0.011293
C	-6.029609	-1.823649	-0.270819
C	-4.8619	-2.547423	-0.058627
N	-8.473516	-1.654154	-0.199327
N	8.051825	-0.933869	0.03308
C	9.120997	-0.778276	0.948837
C	8.293457	-0.095462	-1.074401
C	-9.647236	-2.136463	-0.823629
C	-8.715441	-0.328051	0.229321
C	10.039974	0.166888	0.420667
C	11.178868	0.514363	1.15671
C	11.404625	-0.064877	2.412339
C	10.460783	-0.985991	2.921411
C	9.315919	-1.350887	2.209083
C	7.553471	0.082939	-2.249359
C	8.039176	0.968183	-3.209434
C	9.256453	1.67517	-3.02951
C	9.97956	1.487393	-1.835863
C	9.516483	0.598444	-0.864671
C	-9.89222	-3.361884	-1.447865
C	-11.160363	-3.57611	-1.991674
C	-12.177556	-2.597284	-1.935515
C	-11.896805	-1.355761	-1.349076
C	-10.635662	-1.116531	-0.792288
C	-10.043596	0.032114	-0.127167
C	-10.535058	1.297618	0.213708
C	-9.722585	2.202116	0.910684
C	-8.415303	1.807011	1.273832
C	-7.898225	0.550709	0.947367
Si	-12.039377	11.653746	1.90839
Si	-13.048996	9.98141	-0.725211
Si	-8.954333	10.687045	1.321584
Si	-12.525346	9.017604	3.779854
Si	-9.97782	9.026206	-1.305352
Si	-13.528614	7.330037	1.155818

Si	-9.4457	8.058487	3.203853
Si	-10.460904	6.37429	0.573475
O	-10.369049	11.545622	1.662917
O	-12.467683	10.58657	3.150003
O	-12.781203	11.139689	0.47795
O	-8.805413	9.425812	2.438678
O	-10.927706	8.47105	3.902179
O	-11.566701	9.593315	-1.441711
O	-13.347977	8.021554	2.69114
O	-9.138088	10.01619	-0.222851
O	-13.646543	8.599542	0.048013
O	-10.063875	7.466342	-0.654146
O	-9.720343	6.897187	2.004363
O	-12.140881	6.426119	0.806982
C	-12.55312	13.387432	2.358378
C	-14.235037	10.604892	-2.020109
C	-7.450593	11.785199	1.40006
C	-13.375889	8.990182	5.438025
C	-8.283057	7.417772	4.512446
C	-9.120399	9.023981	-2.960136
C	-9.900373	4.631695	0.145697
C	-13.191202	13.678576	3.50094
C	-14.459014	8.238383	5.68196
C	-13.894334	10.730731	-3.310661
C	-6.437055	11.562693	2.249054
C	-8.63857	7.30033	5.799933
C	-7.999455	9.7216	-3.193648
C	-10.222592	3.593539	1.252923
C	-15.036839	6.235838	1.093942
C	-14.976036	4.926082	0.815047
Si	18.183816	-1.998324	3.794375
Si	15.373457	-0.331616	3.904724
Si	18.411806	-1.856068	7.063037
Si	19.839967	0.825867	3.567073
Si	15.586995	-0.186835	7.174018
Si	17.027111	2.496439	3.707135
Si	20.077503	0.949368	6.830676
Si	17.258391	2.618249	6.971309
O	18.403091	-2.327577	5.438491
O	19.25337	-0.749477	3.394508
O	16.601395	-1.444644	3.559507
O	19.520301	-0.59155	7.250872
O	20.37115	0.988321	5.167547
O	15.071096	-0.368554	5.57087
O	18.565354	1.907993	3.318521
O	16.864799	-1.267149	7.412099
O	15.936895	1.217435	3.51117
O	16.168913	1.388729	7.375903
O	18.831951	2.041705	7.181329

O	17.026891	2.96577	5.330715
C	18.486169	-3.513941	2.753011
C	13.811813	-0.730626	2.937391
C	18.872128	-3.273387	8.181724
C	21.217345	1.175038	2.361297
C	21.632457	1.380019	7.763518
C	14.191366	-0.503547	8.36801
C	16.986391	4.131133	8.025319
C	17.55219	-4.036059	1.945354
C	21.17741	2.197638	1.495082
C	12.654547	0.267481	3.206192
C	19.9519	-3.245905	8.975891
C	22.77746	1.706095	7.14664
C	13.772705	0.414762	9.250596
C	17.952427	4.66328	8.787832
C	16.566468	3.944592	2.627686
C	16.32928	5.167951	3.122621
Si	5.541611	2.018005	-10.042167
Si	8.791642	2.251118	-9.764738
Si	5.312302	1.445565	-6.810555
Si	5.828296	-1.190632	-10.597572
Si	8.565049	1.705314	-6.532509
Si	9.083607	-0.96862	-10.279466
Si	5.562575	-1.76445	-7.381112
Si	8.813626	-1.526062	-7.063995
O	5.15259	2.004027	-8.395498
O	5.387352	0.442058	-10.638768
O	7.162714	2.484907	-10.16153
O	5.112864	-0.23578	-6.807309
O	5.41613	-1.777338	-9.06355
O	8.902751	2.297314	-8.079734
O	7.50264	-1.308602	-10.783029
O	6.885338	1.801345	-6.291323
O	9.258302	0.713439	-10.294221
O	8.955814	0.0604	-6.505994
O	7.189036	-1.990171	-6.974976
O	9.271355	-1.523657	-8.695417
C	4.427344	3.168421	-10.994741
C	9.870359	3.547005	-10.558863
C	4.055937	2.225408	-5.674093
C	4.966524	-2.154069	-11.940244
C	4.492661	-3.099149	-6.640172
C	9.56802	2.732729	-5.348004
C	9.865224	-2.69874	-6.068268
C	3.668648	2.755454	-12.019996
C	5.634258	-2.85569	-12.86745
C	10.88473	3.238954	-11.379561
C	3.099913	1.516485	-5.056922
C	3.7628	-3.938418	-7.38905

C	9.800351	2.612776	-4.021832
C	9.368538	-3.800689	-5.488267
C	10.334357	-1.78551	-11.393924
C	11.205196	-2.703555	-10.950343
C	-1.128758	-9.254695	1.813244
N	-2.15023	-9.830845	1.925519
C	1.31223	-9.156999	1.864378
N	2.369178	-9.652987	2.021518
H	-18.804106	-6.508015	2.358909
H	-15.699793	-5.981555	6.458574
H	-16.569464	-10.964592	0.978035
H	-15.589679	-3.401895	-1.805929
H	-14.762953	-2.256463	-0.750554
H	-13.023392	-7.966392	-3.416018
H	-13.28322	-10.573714	5.219075
H	-8.438046	-7.304473	2.616429
H	-19.886228	-4.77587	0.972753
H	-18.242383	-4.299337	0.277246
H	-13.516975	-3.793033	-3.112082
H	-13.923789	-2.080021	-3.090295
H	-14.710622	-4.027879	7.598681
H	-13.61682	-3.724833	6.140739
H	-16.094662	-12.045538	-1.189628
H	-14.828839	-10.752931	-1.562974
H	-10.669416	-8.290921	-4.069625
H	-10.130163	-7.916831	-2.344743
H	-10.95295	-11.360528	5.42863
H	-10.414646	-10.121474	4.169567
H	-7.21235	-8.260266	0.70175
H	-8.753387	-8.226181	-0.312046
H	-11.929601	-1.82581	2.956779
H	-9.532197	-1.749439	3.51649
H	-9.393518	-3.565626	3.214419
H	-2.152824	-7.009795	1.210659
H	2.174938	-6.82881	1.302465
H	-2.168713	-3.282031	0.23015
H	1.910655	-3.105424	0.332018
H	3.847149	-5.394863	1.040118
H	-3.918787	-5.699555	0.99488
H	3.531483	-1.702909	0.03208
H	5.48671	-0.241675	-0.244121
H	8.101915	-3.524263	0.699954
H	6.139611	-4.988998	1.031092
H	-6.235829	-5.45325	1.066877
H	-8.303278	-4.159631	0.739657
H	-5.981047	-0.821663	-0.680479
H	-3.910155	-2.084612	-0.296315
H	11.885574	1.239497	0.762554
H	10.627772	-1.418208	3.904034

H	8.60122	-2.045149	2.634536
H	6.623875	-0.445944	-2.420118
H	7.44364	1.14133	-4.096984
H	10.910529	2.026332	-1.68418
H	-9.132951	-4.131268	-1.511185
H	-11.376975	-4.530705	-2.459375
H	-12.660836	-0.583185	-1.321845
H	-11.550885	1.578509	-0.0514
H	-7.794374	2.501375	1.833032
H	-6.899062	0.271311	1.259111
H	-12.314513	14.173572	1.644465
H	-15.235516	10.872475	-1.685348
H	-7.424159	12.636336	0.721972
H	-12.954251	9.618372	6.22083
H	-7.283055	7.133352	4.189525
H	-9.568325	8.421397	-3.748331
H	-10.37269	4.34024	-0.800228
H	-8.819707	4.665214	-0.03962
H	-13.488566	14.694087	3.753218
H	-13.440041	12.908727	4.226233
H	-14.94816	8.228115	6.653574
H	-14.89591	7.604312	4.915271
H	-14.593394	11.0979	-4.058897
H	-12.900584	10.470883	-3.665049
H	-5.565032	12.211758	2.290008
H	-6.445442	10.721798	2.937164
H	-7.953399	6.92403	6.556502
H	-9.631553	7.577252	6.143406
H	-7.505193	9.712926	-4.162692
H	-7.534704	10.327135	-2.420321
H	-9.772494	3.928011	2.195631
H	-11.307398	3.56942	1.414688
H	-15.996054	6.710569	1.293279
H	-15.865318	4.300569	0.780614
H	-14.030856	4.431356	0.608734
H	19.47067	-3.972448	2.825253
H	14.065862	-0.737764	1.870368
H	13.502839	-1.75076	3.196421
H	18.221028	-4.145428	8.166649
H	22.074797	0.504811	2.38302
H	21.57946	1.358955	8.850691
H	13.719305	-1.483532	8.32732
H	15.995062	4.580376	7.999946
H	17.740088	-4.921591	1.342197
H	16.563086	-3.594731	1.85856
H	21.98677	2.393071	0.794996
H	20.330306	2.876986	1.45479
H	12.993341	1.280261	2.956928
H	12.426199	0.266289	4.279145

H	20.212809	-4.079565	9.624166
H	20.615419	-2.385948	9.005168
H	23.680125	1.957244	7.699408
H	22.851984	1.733458	6.062934
H	12.959312	0.218763	9.945835
H	14.232089	1.397641	9.310371
H	17.784827	5.547633	9.398763
H	18.94871	4.231367	8.827444
H	16.496114	3.760709	1.556993
H	16.062738	6.007688	2.484458
H	16.394358	5.373087	4.187697
H	4.415051	4.211942	-10.68556
H	9.644577	4.586565	-10.328323
H	4.123111	3.302132	-5.529152
H	3.878165	-2.129174	-11.946862
H	4.483228	-3.181129	-5.55459
H	10.096144	3.528433	-5.871547
H	10.920806	-2.452202	-5.96994
H	3.023306	3.435938	-12.571199
H	3.667188	1.718932	-12.345936
H	5.122814	-3.416283	-13.646916
H	6.720118	-2.894104	-12.87908
H	11.509375	4.002808	-11.83755
H	11.126523	2.20805	-11.623331
H	2.368273	1.982891	-4.400508
H	3.013599	0.441394	-5.190005
H	3.14458	-4.717562	-6.948372
H	3.759813	-3.876151	-8.473843
H	10.526351	3.307657	-3.59409
H	9.991731	-4.479198	-4.909797
H	8.317182	-4.062874	-5.569972
H	10.334204	-1.48725	-12.440943
H	11.931295	-3.176291	-11.60819
H	11.221963	-3.01556	-9.909626

Table S4. Comparison of Au(III) sensing and capacity of various adsorbents.

Material	Au(III) Capacity (mg g^{-1})	Equilibrium time(min)	Gold concentration	Removal	Regeneration	Selectivity	Ref
PCSs@chitosan	3354.92	5	200 ppm	>99%	√	√	This work
PCS-CZ-B-DCM	2203.60	20	200 ppm	>99%	√	√	This work
JNM-100-AO	954.31	3	20 ppm	99%	√	√	3
PCS-ST	670	240	12 ppm	99%	√	√	4
PCS-STOH	1720	900	12 ppm	99%	√	√	4
Tp-BTD-AA	3094.6	360	100 ppm	99%	√	√	5
POSS-2	1486.5	300	2000 ppm	75%	**N.R.**	√	6
DDTD-MOF	1119	600	200 ppm	99%	√	√	7
UiO-66-NH2	495	180	100 ppm	**N.R.**	√	√	8
PCS-PAA	647	30	220 ppm	**N.R.**	**N.R**	√	9
UiO-66-TU	326	180	150 ppm	**N.R.**	**N.R**	√	10

N.R. = Not reported.

Table S5. Consumption for the synthesis of 1 g PCSs@chitosan. (Laboratory research, small dose feeding).

Raw Materials	Amount	Units/ FU	Unit price (USD)	Cost (USD/g)	Brand
Synthesis of 4-carbazolo-phenyl aldehyde					
9H-Carbazole	0.184	g	0.203	0.037	Macklin
4-Bromobenzaldehyde	0.255	g	0.110	0.028	Bide Pharmatech Ltd.
CuI	0.035	g	0.409	0.014	Adamas
K_2CO_3	0.102	g	0.020	0.002	Bide Pharmatech Ltd.
DMF	5.27	g	0.149	0.787	Innochem
Ethyl acetate	55.4	g	0.022	0.122	Fuyu Chemical
n-Hexane	2276.18	g	0.015	3.525	Fuyu Chemical
Electricity (for stirrer and heating)	0.2254	kWh	0.076	0.017	
Synthesis of CZ-B-DCM					
2-(2,6-dimethyl-4H-pyran-4-ylidene)-malononitrile	0.06	g	12.294	0.738	Energy Chemical
CH_3CN	80	g	0.003	0.280	China National Medicines Corporation Ltd.
Piperidine	0.35	g	0.120	0.042	China National Medicines Corporation Ltd.
Electricity (for stirrer and heating)	0.1276	kWh	0.076	0.010	
Synthesis of PCS-CZ-B-DCM					
OVS	0.3	g	1.469	0.441	Energy Chemical
$AlCl_3$	0.3	g	0.056	0.017	J&K Scientific
1,2-Dichloroethane	11.94	g	0.009	0.105	China National Medicines Corporation Ltd.
Ethanol	253	g	0.001	0.354	Fuyu Chemical
Tetrahydrofuran	225	g	0.004	1.007	Fuyu Chemical
Chloroform	135	g	0.010	1.343	China National Medicines Corporation Ltd.
Acetone	253	g	0.008	1.957	China National Medicines Corporation Ltd.
Methanol	253	g	0.004	1.119	Fuyu Chemical

Dichloromethane	151	g	0.003	0.422	Fuyu Chemical
Electricity (for stirrer and heating)	0.2574	kWh	0.076	0.139	
Synthesis of Chitosan-SH					
Chitosan	0.8	g	0.121	0.019	Bide Pharmatech Ltd.
3-Mercaptopropionic acid	0.8	g	0.123	0.098	MREDA
1-ethyl-3-(3-dimethylaminopropyl) carbodiimide hydrochloride	50	g	0.392	19.586	Bide Pharmatech Ltd.
HCl	2.4	g	0.008	0.020	China National Medicines Corporation Ltd.
NaOH	4.3	g	0.002	0.008	Fuyu Chemical
Dialysis membrane	0.6	meter	1.902	1.142	
Water	3000	g	0.0003	0.839	
Synthesis of PCSs@chitosan					
HMPP	0.21	g	0.014	0.003	Bide Pharmatech Ltd.
HOAc	0.17	g	0.006	0.001	China National Medicines Corporation Ltd.
Water	15.15	g	0.0003	0.004	
Electricity (for freeze dryer)	0.1336	kWh	0.076	0.010	
Electricity (for pump)	0.04493	kWh	0.076	0.003	
Total Cost (raw materials + electricity): 34.239 USD					

Note: The average price of electricity in Jinan is 0.076 USD/kWh.

References

S1 L.G. Ding, B.J. Yao, F. Li, S.C. Shi, N. Huang, H.B. Yin, Q. Guan, Y.B. Dong, *J. Mater. Chem. A* 2019, **7**, 4689-4698.

S2 L. Yang, M. Gun, Z. Bian, J. Xie, T. Chen, C. Huang, *Thin Solid Films* 2006, **500**, 224-230.

S3 J. Luo, X. Luo, M. Xie, H.Z Li, H. Duan, H.G. Zhou, R.J. Wei, G.H. Ning, D. Li, *Nat. Commun.* 2022, **13**, 7771.

S4 Q. Ge, H. Liu *Chem. Eng. J.* 2023, **462**, 142323.

S5 S. Yang, T. Li, Y. Cheng, W. Fan, L. Wang, Y. Liu, L. Bian, C.H. Zhou, L.Y. Zheng, Q.E. Cao, *ACS Sustainable Chem. Eng.* 2022, **10**, 9719-9731.

S6 Z. Chen, D. Wang, S. Feng, H. Liu, *ACS Appl. Mater. Interfaces* 2021, **13**, 23592-23605.

S7 Z. Huang, M. Zhao, C. Wang, S. Wang, L. Dai, L. Zhang, L. Xu, *Chem. Eng. J.* 2020, **384**, 123343.

S8 S. Lin, H.K. Reddy, J.K. Bediako, M.H. Song, W. Wei, J.A. Kim, Y.S. Yun, *J. Mater. Chem. A* 2017, **5**, 13557-13564.

S9 Q. Ge, H. Liu, *ACS Appl. Nano Mater.* 2022, **5**, 9861-9870.

S10 Wu, X. Zhu, Z. Wang, J. Yang, Y. Li, J. Gu, *Ind. Eng. Chem. Res.* 2017, **56**, 13975-13982.